Manuscript prepared for Atmos. Chem. Phys.
with version 4.2 of the LaTeX class copernicus.cls.
Date: 30 September 2015

On the radiative impact of aerosols on photolysis rates: comparison of simulations and observations in the Lampedusa island during the ChArMEx/ADRIMED campaign

S. Mailler[1,2], L. Menut[1], A. G. di Sarra[3], S. Becagli[4], T. Di Iorio[3], B. Bessagnet[6], R. Briant[1], P. Formenti[5], J.-F. Doussin[5], J. L. Gómez-Amo[3,8], M. Mallet[8], G. Rea[1], G. Siour[5], D. M. Sferlazzo[9], R. Traversi[4], R. Udisti[4], and S. Turquety[1]

[1]Laboratoire de Météorologie Dynamique, IPSL, CNRS, Ecole Polytechnique, École Normale Supérieure, Université Paris 6, UMR8539 91128 Palaiseau Cedex, France
[2] École Nationale des Ponts et Chaussées - Paristech, Cité Descartes, 6-8 Avenue Blaise Pascal, 77455 Champs-sur-Marne
[3]ENEA, Laboratory for Earth Observations and Analyses, Via Anguillarese 301, 00123 Roma, Italy
[4]Department of Chemistry, University of Florence, Sesto Fiorentino, Florence, 50019, Italy
[5]LISA (Laboratoire Inter-Universitaire des Systèmes Atmosphériques), UMR CNRS 7583, Université Paris Est Créteil et Université Paris Diderot, Institut Pierre Simon Laplace, Créteil, France
[6]National Institute for Industrial Environment and Risks (INERIS), Parc Technologique ALATA, 60550 Verneuil-en-Halatte, France
[7]Dpt. Earth Physics and Thermodynamics, University of Valencia. Dr. Moliner, 50, 46100, Burjassot (Valencia), Spain
[8]Laboratoire d'Aérologie, Observatoire Midi-Pyrénées, 14 Avenue Edouard Belin, 31400 Toulouse, France
[9]ENEA, Laboratory for Earth Observations and Analyses, Contrada Grecale, 92010, Lampedusa, Italy

Correspondence to: Sylvain Mailler, sylvain.mailler@lmd.polytechnique.fr

Abstract. The Mediterranean basin is characterized by large concentrations of aerosols from both natural and anthropogenic sources. These aerosols affect tropospheric photochemistry by modulating the photolytic rates. Three simulations of the atmospheric composition at basin-scale have been performed with the CHIMERE chemistry-transport model for the period from June 6, 2013 to July 15th, 2013 covered by the ADRIMED campaign, a campaign of intense measurements in the western Mediterranean basin. One simulation takes into account the radiative effect of the aerosols on photochemistry, the other one does not.

These simulations are compared to satellite and ground-based measurements, with a particular focus on the area of Lampedusa. Values of the Aerosol Optical Depth (AOD) are obtained from the MODIS instrument on the AQUA and TERRA satellites as well as from stations in the AERONET network and from the MFRSR sun photometer deployed at Lampedusa. Additional measurements from instruments deployed at Lampedusa either permanently or exceptionnally are used for other variables: MFRSR sun photometer for AOD, diode array spectrometer for actinic fluxes, LIDAR for the aerosol backscatter, sequential sampler for speciation of aerosol and Brewer spectrophotometer for the total ozone column. It is shown that CHIMERE has a significant ability to reproduce observed peaks in the AOD, which in Lampedusa are mainly due to dust outbreaks during the ADRIMED period, and that taking into account the radiative effect of the aerosols in CHIMERE improves considerably the ability of the model to reproduce the observed day-to-day variations of the photolysis rate of ozone to O_2 and $O(^1D)$, $J(O^1D)$, and that of NO_2 to NO and $O(^3P)$, $J(NO_2)$. While in the case of $J(O^1D)$ other variation factors such as the stratospheric ozone column are very important in representing correctly the day-to-day variations, the day-to-day variations of $J(NO_2)$ are captured almost completely by the model when the optical effects of the aerosols are taken into account.

Finally, it is shown that the inclusion of the direct radiative effect of the aerosols in the CHIMERE model leads to reduced $J(O^1D)$ and $J(NO_2)$ values over all the simulation domain, which ranges from a few percents over continental Europe and the northeast Atlantic ocean to about 20% close to and downwind from saharan dust sources. The effect on the modelled ozone concentration is twofold, with the effect of aerosols leading to reduced ozone concentrations over the Mediterranean Sea and continental Europe, close to the sources of NO_x, and on the contrary to increased ozone concentrations over remote areas such the Sahara and the tropical Atlantic ocean.

1 Introduction

The Mediterranean region is subject to large aerosol concentrations due to both anthropogenic and biogenic emissions. These large aerosol concentrations affect the radiative transfers in the Mediterranean atmosphere through the direct, semi-direct and indirect effect of the aerosols. Lampedusa, a small island located off the coasts of Sicily and Tunisia, hosts a Station for Climate observation run by the ENEA on its North-Eastern Coast (35.5°N, 12.6°E). At this location, the largest contributors to this effect are the desert dust emissions from the Sahara, the polluted air masses mostly coming from continental Europe, the sea-salt particles emitted either in the Mediterranean Sea itself or advected from the Atlantic, and the particles from biomass burning, when large forest fires occur in southern Europe (Pace et al., 2006). Over the sea surface and in the neighbouring coastal areas, the contribution of sea-spray aerosols is dominant within the boundary layer. These aerosols interact dynamically with meteorology and climate through microphysical and radiative effects (Levy II et al., 2013; Rosenfeld et al., 2014). Apart from these effects on the climate and meteorology, recent studies (Casasanta et al., 2011; Gerasopoulos et al., 2012) have shown that the radiative effect of the aerosols significantly modulates the photolysis rates in the Mediterranean region, focusing on the photolysis rate of ozone to O_2 and $O(^1D)$, $J(O^1D)$, and that of NO_2 to NO and $O(^3P)$, $J(NO_2)$. Casasanta et al. (2011) mention a reduction of 62% in $J(O^1D)$ for a unit Aerosol Optical depth (AOD) at 416 nm when the solar zenith angle (SZA) is 60°. The long-term study of Gerasopoulos et al. (2012), with measurements of $J(O^1D)$ and $J(NO_2)$ for a five-year period above the island of Crete showed that, for a constant solar zenith angle (SZA=60°), $J(NO_2)$ has an annual cycle that reaches about 15% of its average value, and that this annual cycle is essentially driven by the seasonal variations in the composition and optical depth of aerosols. At 60° zenith angle, these authors show that a statistically significant correlation exists between the photolytic rates and the AOD, with a reduction of about 10% in both $J(NO_2)$ and $J(O^1D)$ for an AOD of 0.3 at a zenith angle of 60°, and about 25% for an AOD of 0.7. In particular, mineral dust causes significant absorption in the wavelengths between 300-400 nm, which are determinant in tropospheric photochemistry (Savoie et al., 2000; Diaz et al., 2001; Kaufman et al., 2001). Even though the aerosols impact the tropospheric photochemistry in several ways, including radiative effects as well as heterogeneous chemistry (Bian et al., 2003a), we will focus in this study on the direct radiative impact of aerosols on photolysis rates. It has been shown in the past (Bian et al., 2003b) that this effect modifies the global budgets of O_3 and other gases, and that this effect is twofold, leading to reduction of the ozone concentrations in the troposphere in the high-NO_x, ozone producing regions, and increases of ozone concentrations over the low-NO_x regions, particularly over the oceans.

In order to be able to evaluate and take into account the effect of aerosols on photochemistry over the Mediterranean area, a model for radiative transfer and online calculation of photochemical rates, Fast-JX (Wild et al., 2000; Bian et al.,

2002), which is already used in various CTMs (Telford et al., 2013; Real and Sartelet, 2011) has been included into the CHIMERE chemistry-transport model (Menut et al., 2013). With this new development, the CHIMERE model is able to simulate the radiative impact of aerosols on photochemistry. The Fast-JX module takes into account the values provided in real time by the CTM for all aerosol species as well as for tropospheric ozone up to the top of the CHIMERE domain. The real-time model values of the meteorological variables (temperature, pressure and cloud cover) are also used by the Fast-JX module. Monthly climatological distributions for stratospheric ozone are taken from the McPeters et al. (1997) climatology. As the CHIMERE model takes into account all the major anthropogenic and natural sources of aerosols and trace gases in a realistic way for the Mediterranean basin (Menut et al., 2015), the CHIMERE model including the Fast-JX module, as used in the present study, is an adequate tool to investigate the impact of the aerosols on photochemistry at least for the Mediterranean basin.

In the framework of the ChArMEx (Chemistry-Aerosol Mediterranean Experiment, http://charmex.lsce.ipsl.fr) campaign, a special operation period, ADRIMED (Aerosol Direct Radiative Impact in the Mediterranean), has been conducted during the summer of 2013. Special Operation Period 1a (SOP1a) lasts from June 12 to July 5, covering the central part of the simulated period. Various observational data, including photolysis rates $J(\mathrm{O^1D})$ and $J(\mathrm{NO_2})$ at the Lampedusa supersite, are available for this period, during which various episodes of desert-dust intrusions in the free troposphere above Lampedusa have occured. For the 40 days from June 6, 2013 to July 15th, 2013, two simulations have been performed for an area covering the Mediterranean basin, continental Europe and the northern part of Africa. The first simulation (REF) is described and validated in Menut et al. (2015). It includes emissions from mineral dust, biomass burning, anthropogenic and biogenic sources, as well as the radiative effect of aerosols on photochemistry. A second simulation, which we will refer to as NA (No aerosol radiative effect) is performed with exactly the same meteorology, the same emission for aerosols and trace gases, but artificially cancelling the radiative effect of aerosols by setting the real part of their refractive index to 1 and the imaginary part to 0 in the radiative transfer model, making them perfectly transparent at all wavelengths. Therefore, the differences between these two simulations reflect the direct radiative effect of aerosols on photochemistry in the CHIMERE model.

Section 2 exposes the modelling strategy used in both simulations for meteorology, atmospheric chemistry and the radiative transfers, as well as the observational data and techniques. Section 3 presents the validation of the REF simulation by comparison to AOD observations from satellite as well as from ground stations. Descriptions of the vertical structure and speciation of aerosols above Lampedusa as simulated and as observed by the measurement facilities at Lampedusa are also presented. The simulated photolytic rates $J(\mathrm{O^1D})$ and $J(\mathrm{NO_2})$ from both simulations are also compared to the values observed at Lampedusa in order to find whether taking into account the optical effects of aerosols improve the representation of $J(\mathrm{O^1D})$ and $J(\mathrm{NO_2})$ in the CHIMERE model. That section also contains an evaluation of model sensitivity to the optical depth of aerosols regarding the concentration of ozone over the whole simulation domain. Finally, Section 4 sums up and discusses the results obtained in Section 3.

2 Data and methods

2.1 Models

2.1.1 Meteorology and atmospheric chemistry

Meteorology has been modelled using the WRF model (Weather Research and Forecasting model) (Michalakes et al., 2004), version 3.5.1, as described in Menut et al. (2015), with a horizontal resolution of $60 \times 60\mathrm{km}$ and 28 vertical levels from the surface up to 50 hPa. The surface layer scheme is based on Monin-Obukhov with Carlson-band viscous sublayer, and the Planetary boundary layer physics are processed using the Yonsei University Scheme (Hong et al., 2006). The continental surfaces are treated using the Noah Land Surface Model scheme with four soil temperature and moisture layers (Chen and Dudhia, 2001), and the model uses the cumulus parameterization of Grell and Devenyi (2002).

The meteorological model is forced at its boundaries by the global hourly fields of NCEP/GFS (National Center for Environmental Forecasting/Global Forecast System), and inside the domain the main atmospheric variables (pressure, temperature, humidity and wind) are nudged towards the NCEP/GFS hourly fields using spectral nudging (von Storch et al., 2000) for wavenumbers up to 3 in latitude and longitude, corresponding to wavelengths about $2000\mathrm{km}$. Nudging is not performed below 850 hPa in order to allow the regional model to create its own structures within the boundary layer. Meteorological input fields have been produced for the same domain as the CHIMERE simulation domain, which is shown on Fig. 4.

The reader is referred to Menut et al. (2015) for the further description and validation of this meteorological simulation. These authors indicate a persistant negative bias in temperature over all but one locations: over 13 stations in southern Europe, the temperature bias ranges between $-4.10\mathrm{K}$ and $+0.87\mathrm{K}$ (see their Table 4). Possible causes of this bias include problems in the boundary-layer and microphysics parameterizations. In spite of this large bias and of difficulties of the model to catch the diurnal cycle of the observations, they show that the correlation coefficients of the simulated vs. observed 2m-temperature for this simulations range between 0.87 to 0.99 for the same subset of stations, show-

ing that the temporal evolutions of the temperature are reproduced quite correctly by this meteorological simulation.

For the island of Lampedusa, the WRF fields for temperature and wind module are shown and compared with the field data from the Lampedusa supersite (Fig. 1). As for most other locations (Menut et al., 2015), the modelled temperature has a significant low bias. It also lacks a daily cycle compared to the in-situ data, which has pronounced daytime maxima of the temperature. The lack of a daily cycle is consistent with the fact that, at the model resolution ($60 \times 60\,\mathrm{km}$), the island of Lampedusa is not resolved, so that the modelled values reflects open-sea temperature, which is expected be weaker than temperature over land in summer time, and to have a much weaker diurnal cycle. The temperature bias is in average of about 5K for daily temperature maxima and 3K for daily temperature minima. As we checked that this strong temperature bias is not present in the GFS data used to nudge the WRF model, it is possible that a misconfiguration of the WRF model is the cause of this error. The impact of a 5K underestimation of daytime temperature on $J(\mathrm{NO_2})$ and $J(\mathrm{O^1D})$ photolysis rates can be estimated according to Dickerson et al. (1982). Both $J(\mathrm{NO_2})$ and $J(\mathrm{O^1D})$ values increase with temperature, but the dependancy of $J(\mathrm{NO_2})$ on temperature is much weaker than that of $J(\mathrm{O^1D})$. While $J(\mathrm{O^1D})$ increases by more than 50% when temperature increases from 273 K to 307 K, $J(\mathrm{NO_2})$ does so by less than 5%. Based on the results of Dickerson et al. (1982), the impact of a cold bias of 5 K on $J(\mathrm{O^1D})$ can generate an underestimation of 5 to 10% on $J(\mathrm{O^1D})$ in the temperature range for daytime temperatures during the simulation period (around 295K), and only about 1% on $J(\mathrm{NO_2})$.

Regarding the wind-module, which is a key parameter in modelling sea-salt emissions, Fig. 1b shows that the agreement between model and data for this parameter is quite good, even if for some periods of strong wind, as it is the case from June 23 to June 27 for example, the model tends to underestimate the wind module. The error on wind direction has also been evaluated by comparison to local hourly measurements at Lampedusa. It is found that, when the wind velocity was below the median value of $5.3\,\mathrm{ms^{-1}}$, the error on wind direction is very strong, suggesting that when the synoptic wind velocity is weak, the local wind is dominated by effects such as the land-breeze and sea-breeze, which cannot be represented adequately at the model resolution. On the contrary, when the wind velocity is above $5.3\,\mathrm{ms^{-1}}$, the median of the absolute error on wind velocity is 35.5°, and the error distribution peaks in the vicinity of zero, showing that the synoptic wind patterns are reproduced rather well by the model.

[Fig. 1 about here.]

Atmospheric chemistry has been modelled with the CHIMERE chemistry transport model (Menut et al., 2013). We used the MELCHIOR-2 (ModELe de la CHimie de l'Ozone à l'échelle Régionale 2) chemical mechanism along with the aerosol scheme by Bessagnet et al. (2004). For this study, the emissions are taken from the HTAP (Hemispheric Transport of Air Pollution) inventory provided by the EDGAR (Emissions Database for Global Atmospheric Research) team[1], and adapted to the model grid as described in Menut et al. (2013). The resulting mean NOx emissions over the simulation domain are shown in Fig. 2. The boundary conditions for all gaseous and particulate species are taken from LMDZ-INCA (Laboratoire de Météorologie Dynamique Zoomé - INteraction avec la Chimie et les Aérosols) climatology (Hauglustaine et al., 2004), except mineral dust which is taken from the GOCART2 (Goddard Chemistry Aerosol Radiation and Transport 2) climatology (Ginoux et al., 2001), which gives the dust climatology with 7 size bins instead of 3 for LMDZ-INCA. This simulation includes the representation of forest fire emissions, as described in Turquety et al. (2014). Dust emissions have been simulated as explained in Menut et al. (2015), following the Marticorena and Bergametti (1995) scheme for saltation and Alfaro and Gomes (2001) for sandblasting. All the simulations presented were started from June 1st, 2013, and last until July 15th, 2013. The initialisation was done from the global LMDZ-INCA and GOCART2 climatologies, and 5-day spinup period has been discarded before analyzing the simulation outputs: only the 40 days from June 6 to July 15 will be analyzed in the following.

[Fig. 2 about here.]

Vertical discretization is on 20 levels, with 10 layers below 800 hPa and 10 layers between 800 hPa and the model top, which is placed at 300 hPa. The lowest model layer has 3 hPa thickness, and all the levels between 800 hPa and 300 hPa have equal thickness (60 hPa per layer). This vertical discretization has been chosen to permit a fine representation of both the boundary layer and the free troposphere. The radiative transfers from 300 hPa upward are modelled using climatological ozone concentrations.

The discretization of the particle size distribution of the aerosols is performed over 10 size bins, from 39 nm to 40 $\mu\mathrm{m}$ following a geometric progression with ratio 2, as shown in Tab. 1.

[Table 1 about here.]

2.1.2 Actinic fluxes and photolysis rates

The photolysis rates have been calculated using the Fast-JX model, version 7.0b (Wild et al., 2000; Bian et al., 2002). At each time step and in each grid cell, this model resolves the radiative transfers in the model atmospheric column, computing the actinic fluxes at each model level and integrating them over N wavelength bins in order to produce accurate

[1] http://edgar.jrc.ec.europa.eu/htap_v2

photolysis rates. For our study, N is set to 12, which is the value recommanded by Fast-JX developers for tropospheric studies. These 12 wavelength bins include the 7 standard Fast-J wavelength bins from 291 nm to 850 nm, as described in Wild et al. (2000). The 7 standard Fast-J wavelength bins are essentially concentrated from 291 nm to 412.5 nm which is the spectral band relevant for tropospheric photochemistry. Following the recommandations of Fast-JX model developers, 5 additional wavelengths bands have been used as well, from 202.5 nm to 291 nm, but they are only relevant in the upper tropical troposphere which is not included in the present study since the model top is at 300 hPa. The optical properties of the aerosols are treated at 5 wavelengths : 200 nm, 300 nm, 400 nm, 600 nm and 1000 nm. The optical treatment performed includes absorption by tropospheric and stratospheric ozone, Rayleigh scattering, Mie diffusion by liquid- and ice- water clouds, and absorption and Mie diffusion by aerosols.

The radiative indices for the main aerosol species have been taken as provided on the ADIENT project website[2]. The technical and scientific choices are given in the corresponfing technical report by E. J. Highwood[3]. For mineral dust, they are given in Tab. 2, and taken from the AERONET (AErosol RObotic NETwork) values of Kinne et al. (2003). From these values, the extinction cross section per particle, single-scattering albedo and first 7 terms of the Legendre expansion of the scattering phase-function are calculated using Michael Mischenko's code (Mischenko et al., 2002), assuming log-uniform distribution within each diameter bin, and used as input of the Fast-JX radiative code. As in Bian et al. (2003a), we chose to neglect the influence of relative humidity on the optical properties of mineral dust, which has been shown to have a very small effect on the volume of dust particles (Herich et al., 2009). However, water uptake by hygroscopic species such as nitrates, sulphates and ammonium in subsaturated conditions is represented using the ISORROPIA module (Nenes et al., 1998), as described in Bessagnet et al. (2004). The optical effect of the liquid-phase water generated by the hygroscopic growth of these aerosols is taken into account by the Fast-JX module as a separate aerosol species with the optical characteristics of water. Treatment of clouds by Fast-JX is described in, e.g., Wild et al. (2000); Bian et al. (2002). It is worth noting that the simulation period has been largely dominated by conditions with no cloud cover over Lampedusa. However, the spectrometer measurements show that thin clouds occured on June 6, 7, 10, 11, 13, 14, 24 and on July 4, 5 during daytime above Lampedusa.

The photolysis rates in CHIMERE are updated every 5 minutes by calling the Fast-JX model. The AOD for each model layer is an intermediate result of the Fast-JX model, which we sum over the model layers and export for the 5 wavelengths used by Fast-JX in order to compare it to available observations.

One key parameter in simulating $J(\mathrm{O^1D})$ is the total atmospheric ozone column. Within the simulation domain (from the surface to 300hPa), Fast-JX uses the ozone concentrations calculated within CHIMERE. Above this level, that is, for upper tropospheric and stratospheric ozone, Fast-JX uses tabulated climatological ozone concentrations. These climatological concentrations from McPeters et al. (1997), included within the Fast-JX module in its standard configuration, are given with a vertical resolution of about 2 km up to an altitude of about 60 km, with monthly values for every 10° latitude band. For the latitude band corresponding to Lampedusa (30-40°N), the stratospheric ozone column obtained by vertically summing these climatological concentrations amounts to 248.6 DU for the month of June, and 236.4 DU for the month of July. The contribution of tropospheric ozone from the CHIMERE model is of about 30DU for all the simulation periods. Therefore, the total ozone column taken into account by the radiative transfer model oscillates around 280 DU for the month of June, and 265 DU for the month of July, a value which is far below the measured value above Lampedusa, which evolves within the 300-360 DU range for all the simulation period (Fig. 3). Total ozone is routinely measured at Lampedusa by means of a MKIII Brewer spectrophotometer, as described in Meloni et al. (2005). According to the state-of-the-art measumement values from Ziemke et al. (2011) (their Fig. 9b), for the area of Lampedusa, the climatological values for the stratospheric ozone column should be of 280 DU for June and 260 DU for July at Lampedusa, much stronger than the McPeters et al. (1997) values used in the present study (respectively 248.6 DU and 236.4 DU for June and July). Therefore, the low bias of about 30 DU in our total ozone columns relative to observed values can be attributed mostly or entirely to the use of the climatology used in the present study for stratospheric ozone values. This insufficient stratospheric ozone column is expected to have a significant impact on the modelled $J(\mathrm{O^1D})$ photolytic rates.

Figure 3 also shows that the variability of the total ozone column is much smaller in the model than in the observed values, most likely also due to the use of climatological stratospheric ozone colums, because the observed extreme variations of the ozone column (from 360 DU to 290 DU) are too strong to be due to the variability of the tropospheric ozone column alone. In fact, the ozone column simulated by CHIMERE from the ground to 300hPa varies around 25 DU, with relatively small variations. This value of tropospheric ozone column is smaller than climatological value from the Ziemke et al. (2011) results, which is around 40 DU for June-July in the Lampedusa area, but this is consistent with the fact that the atmospheric layer from the ground to 300hPa simulated by CHIMERE does not include the ozone-rich layers of the upper troposphere.

As it is well known that the total ozone column is a criti-

[2] http://www.reading.ac.uk/adient/refractiveindices.html

[3] http://www.reading.ac.uk/adient/REFINDS/Techreportjul09.doc

cal parameter in simulating accurately the value of $J(O^1D)$ in the troposphere, we performed a sensitivity simulation (which we wille refer to as O3+) identical to the REF simulation except that the calculation of the photolytic rates has been performed after multiplying the ozone concentrations throughout the stratosphere and the troposphere by 1.18, thereby compensating the bias on ozone column visible on Fig. 3.

[Fig. 3 about here.]

[Table 2 about here.]

2.2 The backplume calculation methodology

In order to understand the origin of several air masses, a simplified backplume model was developed and used in this study. The main principle is to use the WRF simulation results and to advect back in time numerous passive tracers. For each backplume, a location, a time and an altitude is chosen. The meteorological parameters used are:

- The three-dimensional wind components: u the zonal wind (m s^{-1}), v the meridian wind (m s^{-1}) and w the vertical wind (m s^{-1}).
- The boundary layer height $\overline{h}$ and the surface sensible heat flux Q_0.

For each starting point, one hundred passive tracers are launched. For each one, its back-trajectories are estimated during the previous 120 hours, back in time. Three cases are considered for each time and each location:

- In the boundary layer and during a convective period ($Q_0 > 0$): we consider that the particle is in the convective boundary layer. The meteorological fields being available at an hourly time-step, we consider the particle may have been at any level inside the boundary layer the hour before. We thus apply a random function to reproduce vertical mixing within the boundary layer.
- In the boundary layer and during a stable period ($Q_0 < 0$): the particle stays in the boundary layer at the same altitude
- In the free troposphere: we consider that the particle vertical evolution may be influenced by the vertical wind component. We thus apply a random function to estimate its possible vertical motion with values between $w/2$ and $3w/2$.

Particles launched at the same initial position can have distinct evolutions back in time: therefore, the initial sample of 100 particles have distinct backtrajectories depending on their random vertical movements inside the convective boundary layer, and their parlty random vertical movements within the free troposphere. Even though this backplume model is possibly not comparable to state-of-the-art models such as HYSPLIT or FLEXPART, this model has been chosen for its simplicity of use in a study in which backtrajectories are not a critical part. It does not necessarily imply that such a simplified formulation would be adequate for studies in which accuracy of the backplume simulations is critical.

2.3 Observational data and techniques

The Lampedusa station is located on the Lampedusa island. Lampedusa is a small island located some 140km East of the Tunisian coast and about 210km South-West of the Sicilian coast, so that the aerosol properties at and above Lampedusa can be considered as mainly representative of long-range transport and of marine aerosol (Pace et al., 2006). The measurements available at Lampedusa during the simulated period or at least during part of it include measurements by the MFRSR instrument (Multi Filter Rotating Shadowband Radiometer) for the Aerosol optical depth, a Metcon diode array spectrometer for actinic flux and photolytic rates, a Brewer spectroradiometer for total ozone column, an aerosol LIDAR, and a low-volume dual-channel sequential sampler.

2.3.1 Remote sensing and radiative measurements

The AERONET (Aerosol Robotic Network, http://aeronet.gsfc.nasa.gov) and MFRSR data was used for the AOD, MFRSR data was also used for calculating $J(NO_2)$ and $J(O^1D)$ at the Lampedusa supersite. The AERONET data was used for three stations : Lampedusa (35.51°N ; 12.63°E), Oujda (34.65°N ; 1.90°E) and Palma de Mallorca (39.55°N ; 2.63°E). Level 2.0 data was used for Oujda and Palma de Mallorca, while only Level 1.5 data was available for Lampedusa. The AOD time series for Lampedusa was completed by MFRSR measurements carried out at the Lampedusa station (Pace et al., 2006; di Sarra et al., 2015) for the periods when the AERONET data were not available, namely June 6 to June 16, and June 27. It was shown in di Sarra et al. (2015) that the mean bias of the MFRSR AOD relative to the AERONET measurements is always smaller than 0.004 for long-term series (1999-2013), with a r^2 correlation coefficient always above 0.97 at all wavelengths between the AERONET and the MFRSR measurements. The very good correspondance between both time series make it possible to use the MFRSR measurements to complete the AERONET time series, as done in the present study. The AERONET AOD as well as MFRSR AOD have been interpolated at the wavelength of 400 nm, which is one of the five wavelengths for which Fast-JX computes the AOD. The interpolation was performed following an Angström power law., based on the nearest available wavelengths in the measured data, 380 nm and 440 nm for the AERONET data, 416 nm and 440.6 nm for the MFRSR data.

Actinic flux spectra were measured using a Metcon diode array spectrometer (Casasanta et al., 2011). The actinic flux

measurements were calibrated at the beginning of SOP1a by using NIST traceable 1000 Watt lamps. The value of $J(\mathrm{O^1D})$ was derived from the actinic flux measurements as described by Casasanta et al. (2011). $J(\mathrm{NO_2})$ was calculated from the measured actinc flux spectra by using the temperature dependent NO_2 absorption cross sections by Davidson et al. (1988) and the NO_2 quantum yield from Gardner et al. (1987). It is worth noting that the measured actinic flux, and therefore the photolysis rates, take into account only the downward actinic flux.

The estimated accuracy is about 0.01 for the AERONET AOD, about 0.02 for the MFRSR AOD (Pace et al., 2006), and about 1% on the total ozone measurements by the Brewer spectroradiometer, which are done routinely at Lampedusa. The estimated uncertainty is between 5 and 8% for $J(\mathrm{O^1D})$, depending on the solar zenith angle and occurring conditions, and about 3-4% for $J(\mathrm{NO_2})$.

An aerosol LIDAR is operational at Lampedusa, and provides measurements of vertical profiles of the aerosol backscattering at 532 nm. Details on the instrumental setup and on the retrieval method are given by Di Iorio et al. (2009). For this study, one or two daily backscattering profiles, obtained by averaging LIDAR signal over 5-30 minute intervals, are chosen as representative for the occurring conditions on the corresponding day. The vertical resolution of the measurements is 7.5 m.

The AOD from MODIS Aqua and Terra v. 5.1 at 550nm has been retrieved using the NASA LADS website[4]. Only quality-assured, cloud-screened level 2 data has been used for this study. The expected error envelope for these values are of $\pm 0.05 + 0.15 AOD$ over land, and $\pm 0.03 + 0.05 AOD$ over ocean. About 60% of values (above ocean) and 72% (over land) fall within this expected error margin (Remer et al., 2008). When available, we use in priority the AOD from the deep-blue algorithm, which permits to have satellite-retrieved values for the AOD even over bright surfaces such as desertic areas. This product has an expected error envelope of $\pm 0.03 + 0.20 AOD$ (Sayer et al., 2013)

2.3.2 Aerosol concentration and speciation

$\mathrm{PM_{10}}$ samples were collected at Lampedusa Island at 12-hour resolution by using a low volume dual channel sequential sampler (HYDRA FAI Instruments) equipped with sampling heads operating in accord with the European Norm EN12341 (following Directive 2008/50/EC on ambient air quality and cleaner air for Europe). The mass of $\mathrm{PM_{10}}$ was determined by weighting the filters before and after the sampling with an analytical balance in controlled conditions of temperature (20 ± 1 °C) and relative humidity (50 ± 5 %). The estimated error on the basis of balance tolerance for the $\mathrm{PM_{10}}$ mass is around 1% at 30 $\mu \mathrm{g m^{-3}}$ of $\mathrm{PM_{10}}$ in the applied sampling conditions. A quarter of each filter is analysed for soluble ions content by Ion Chromatography as described in Marconi et al. (2014). The error margin for Ion Chromatographic measurements is of 5% for all the considered ions.

Na, Cl, Mg, Ca, K and sulphate are the main components of sea-salt aerosol (SSA). As these ions (excluding Cl) have other sources than sea-spray, the sea-salt (ss) fraction of each ions was used to SSA calculation. details on the calculation of sea-salt and non-sea-salt (nss) fraction for Na and Ca by using the ratio Ca/Na in sea water ($(\mathrm{Ca/Na})_{\mathrm{sw}} = 0.038$; (Bowen, 1979)) and Na/Ca average in the upper continental crust ($(\mathrm{Ca/Na})_{\mathrm{ucc}} = 0.56$; (Bowen, 1979)) are reported in Marconi et al. (2014). The sea-salt fractions for Mg, Ca, K and sulphate are calculated by multiplying the ssNa by the ratio of each component in bulk sea water: $(\mathrm{Mg/Na})_{\mathrm{sw}} = 0.129$, $(\mathrm{Ca/Na})_{\mathrm{sw}} = 0.038$, $(\mathrm{K/Na})_{\mathrm{sw}} = 0.036$, $\left(\mathrm{SO_4^{2-}/Na}\right)_{\mathrm{sw}} = 0.253$ For chloride we used the measured concentration instead of the calculation from ssNa, because during the aging of sea spray chloride undergoes a depletion process (Keene et al., 1998), mainly due to reactions with anthropogenic H_2SO_4 and HNO_3, leading to re-emission of HCl in the atmosphere. Previous work by Kishcha et al. (2011) shows a very good agreement between SSA obtained by DREAM-Salt model and the calculated SSA from chemical composition at Lampedusa.

Dust aerosol is calculated from nssCa as this marker is one of the most reliable of crustal material (Putaud et al., 2004; Sciare et al., 2005; Guinot et al., 2007; Favez et al., 2008). Besides, Ca is largely used because it allows the identification and quantification of Saharan dust on the basis of only ion chromatographic measurements. On the other hand, upper continental crust presents a large variability in Ca content. In particular, some areas of the Sahara are enriched in Ca minerals (Scheuvens et al., 2013), leading to an overestimation of crustal material in the aerosol by using only the Ca (or nssCa) in the calculation. In the Mediterranean region, several studies have evaluated and used calcium-to-dust conversion factors to estimate the crustal content (Sciare et al., 2005; Favez et al., 2008). In Lampedusa, over an extensive dataset, (Marconi et al., 2014) found a significant correlation between nssCa and crustal content computed by the more reliable method of the main crustal element oxides formula. The slope of the regression line (10.0 ± 2 %), which is in the range of previous studies in the Mediterranean region (Sciare et al., 2005; Favez et al., 2008) is used as calcium-to-dust conversion factor in the present study. Finally, non-dust $\mathrm{PM_{10}}$ is obtained by subtraction of dust content from $\mathrm{PM_{10}}$ total mass.

3 Results

[4] ftp://ladsweb.nascom.nasa.gov/allData/51/

3.1 Representation of the aerosols in the model: comparison to observations

3.1.1 Aerosol optical depth

[Fig. 4 about here.]

Figure 4 compares the AOD simulated by CHIMERE at 550 nm (interpolated from the simulated values at 400 and 600nm following an Angström power law) to that measured by MODIS at 550 nm, averaged from June 6 to July 15. It shows that, on average for all the considered period, CHIMERE realistically reproduces the main features of the AOD over the considered region, with average values above unity for the Sahelian band and the Arabian peninsula. However, CHIMERE misses high AOD values on the eastern side of the Caspian Sea as well as over the northern part of the Atlantic, and also underestimates the AOD in eastern Sahara. For the first area, the underestimation of the AOD by CHIMERE may be related to missing dust emissions, while for the northern Atlantic the high AOD values in MODIS are related to an average computed from very few data points, possibly during an event of transport of an aerosol plume (e.g. biomass burning or mineral dust) from outside the simulation domain, or contaminated by the presence of thin clouds in that area.

For the most important part of our domain, including continental Africa, the comparison of the average AOD between CHIMERE and MODIS is rather satisfactory: maxima due to local dust emissions are observed in the Sahara and Sahel, and the climatological dust plume off the coast of West-Africa and above the Capo Verde islands is well captured by the model, even though some underestimation in the model can be seen in this plume.

Over the Mediterranean Sea, average values around 0.2 are modelled by CHIMERE and observed by MODIS, with larger values just off the coasts of North-Africa and a south-north gradient, with smaller AOD values in the northern part of the Mediterranean sea.

[Fig. 5 about here.]

Regarding the time evolution of the AOD, we selected three particular days in June: June 17, 19 and 21, sampling the dust outbreak that occured between June 13 and June 25 over the Western Mediterranean basin, during ADRIMED SOP1a. Figure 5 shows the AOD at 400 nm and at 12 GMT simulated by CHIMERE for these three days, and measured by MODIS for the same dates (MODIS overpass was between 10 GMT and 14GMT over the considered zones for these days).

For June 17 (Fig. 5a-b), the dust plume is visible both in the model and in observations, with maximal AOD values around 0.6 in both cases, even though the plume seems slightly more extended and optically thicker in the model than in the observations. In both model and observations, the maximal AOD for this plume is located over the sea, south-west of the Balearic islands. For June 19 (Fig. 5c-d), the dust plume has moved to the east, just west of Corsica and Sardinia. It extends further to the south in the model than in observations. Finally, on June 21 (Fig. 5e-f), the dust plume is over the Tyrrhenian Sea, also reaching Lampedusa, and has become significantly more intense in the model than in observations.

During the same time period, a zone of strong AOD is present in CHIMERE off the coasts of France, Britain and Ireland (Fig. 5a), then over the Gulf of Gascony (Fig. 5c) and finally on June 21, a zone of very strong AOD over the North Sea. No MODIS measurements are present at the same time to evaluate this zone of high aerosol loads, even though Fig. 5d indicates a zone of relatively strong AOD over the North Sea at that time (June 19), consistant with CHIMERE simulation.

A detailed comparison of the AOD with AERONET stations for all the ADRIMED period is presented in Menut et al. (2015). In the present study, we selected three AERONET stations that have sampled the dust plume we discussed before in order to evaluate the modelled AOD for the considered period.

[Fig. 6 about here.]

[Table 3 about here.]

These three AERONET stations have been selected in the Western mediterranean according to the data availability for June 2013 and their position on the trajectory of the dust plume of June 13-25 as seen by MODIS. As discussed in Section 2, the three selected stations are Lampedusa (Italy), Oujda (Marocco) and Palma de Mallorca (Spain). The AERONET data for Lampedusa was not available for June 1st to June 16, so that the time series have been completed using the MFRSR data at Lampedusa station for those 16 days as well as for June 27. The comparison of the AOD measured in these three AERONET stations to the AOD of CHIMERE is shown on Fig. 6 at 400 nm. Statistical scores have also been calculated for 10 additional AERONET stations from the Saharian area to northern Europe (Table 3).

The dust peak observed from June 21 to 24 in Lampedusa is simulated realistically by CHIMERE (Fig. 6a). The peak value of the AOD is about 0.5 in the model and 0.35 in the observations. Three other sharp peaks in AOD are represented in CHIMERE for June 6, June 9-10 and July 2-4. The peak of June 6 is the most intense in the simulation period, and has a rather short duration (about 24 hours). The maximal value of the AOD during this peak is between 0.8 and 0.9 in both the MFRSR data and the model in the afternoon of June 6. The AOD value then steadily decreases on June 7, ranging between 0.5 and 0.3 in both modelled and measured values for that day. The peak in the afternoon of June 9, the second most intense in the whole data series (AOD=0.6) has been

sampled by MFRSR, and is present as well in CHIMERE, with a very comparable peak value, reached in the afternoon of June 9 and the following night. The decrease of the AOD values occurs on June 10, when AOD returns to a value of about 0.2. A last peak in AOD is present in both model and observations from July 2 to July 4, followed by moderate AOD values, around 0.2, throughout the rest of the simulation period. For the entire simulation period at Lampedusa, the correlation coefficient between simulated and observed values is of 0.8, while the bias of the model compared to the observations is of 19%.

For the Oujda station (Fig. 6b), a period of strong AOD is represented in both the model and observations from June 12 to June 17, with a similar timing and duration between the model and the observations and a stronger value for the maximal AOD in the model than in observations (0.6 vs 0.4). Another strong AOD peak is simulated by CHIMERE from June 28 to July 2, but with no available data at the time, and a last AOD peak is modelled and observed on July 11-12. The background value of the AOD (about 0.05-0.1) for this location is represented realistically by CHIMERE. For this station, and for the entire simulation period, the correlation coefficient between the simulated and observed values is of 0.64, with a negative bias of -9.9% of the observed values relative to the simulated ones.

Finally, for the Palma de Mallorca station (Fig. 6c), a very brief peak in AOD is simulated in CHIMERE for Jun 7, but not seen in the AERONET time series because it occurs in nighttime. Thereafter, a peak from June 16 to June 18 with AOD reaching 0.5 in CHIMERE and 0.3 AERONET is simulated and observed. A significant AOD peak from 25-30 June is observed but missed by the model. A last AOD peak is simulated and observed on July 2-3, and a trend towards higher AOD values can be seen in both the model and observations towards the end of the period. Contrary to Oujda and Lampedusa, the model behaviour is however globally not satisfactory at Palma de Mallorca, with a correlation coefficient of only 0.18 between simulated and observed AOD values (Table 3).

If we now briefly examine the statistical scores of the model for the 12 stations that have been selected for the statistical analysis in Table 3, several observations can be made. Regarding the average AOD bias, it is generally moderate for the 10 first stations of the list, in Africa and the Mediterranean basin (from -35% to +19%), but not for the two stations of Mainz (Germany) and Palaiseau (France), in continental Europe (-61% and -45% respectively). This confirms the observation made above from comparison with satellite data that the model has problems reproducing the relatively high AOD values that are observed over continental Europe. The same is true for the time evolution of the AOD: while the correlation coefficients for all the stations in Africa and the Mediterranean basin are significant at 99% except for the stations of Potenza (Italy) and Cap d'En Font (Baleares), the simulated AOD values have no correlation to the observations at the stations of Palaiseau and Mainz.

All in all, it can be seen that the AOD values simulated by CHIMERE over the western Mediterranean and the Saharan desert compare well to observations from MODIS, AERONET and MFRSR, and that the peaks simulated by CHIMERE during that period are generally observed except when they occur during nighttime, as it is the case for the night of 7-8 June at Palma de Mallorca. However, the AOD peak values during some AOD peaks are overestimated by up to 50% when compared to the observed values. Only one significant AOD peak is observed but missed by the model, from June 25-30 at Palma de Mallorca, while the model catches all the AOD peaks that occur at Lampedusa and Oujda during the simulation period. The longest dust transport event of this period (12-24 June) is represented realistically for all three locations, first in Oujda, therafter in Palma de Mallorca, and finally at Lampedusa, even though for these three locations the peak value of the AOD is stronger in CHIMERE than in the observations. Even though statistical analysis shows that the ability of the model to reproduce the observed AOD variation depends a lot on the location, and is not good over continental Europe, its performance is very satisfactory over Lampedusa, which was one of the ADRIMED SOP1a supersite, including measurements of both $J(\mathrm{O^1D})$ and $J(\mathrm{NO_2})$. Therefore, it is possible to use the present simulations over the period of time from June 6 to July 15, 2013 to examine the impact of aerosol screening on photochemistry, taking advantage of the availability of measurements from the ADRIMED SOP1a period.

3.1.2 Vertical structure

[Fig. 7 about here.]

The episodes of dust incursion visible on the simulated AOD time series (Fig. 6a) can also be seen in the time-altitude simulated particles concentrations, see Fig. 7a for coarse particles ($\mathrm{PM_{10}}$ - $\mathrm{PM_{2.5}}$) and Fig. 7b for fine particles ($\mathrm{PM_{2.5}}$). Dust is present above Lampedusa in the simulation outputs from June 4 to June 10, from June 19 to June 28, from July 1st to July 4, and from July 11 to July 15 (Fig. 7a). A significant amount of finer particles is also present in the boundary layer during most of the simulation period, particularly from June 11 to June 20, while maxima of $\mathrm{PM_{2.5}}$ concentration occur in the free troposphere as well during the dust outbreaks. LIDAR profiles have been selected once or twice a day for comparison to the model (Fig. 7c). In these LIDAR measurements of backscatter coefficient, aerosol plumes in the free troposphere are clearly visible from June 8 to June 10, from June 19 to June 28, and from July 2 to July 4. These aerosol plumes in the troposphere are seen between 2000 and 6000 m altitude, consistent with the altitudes of the $\mathrm{PM_{10}}$ maxima simulated in CHIMERE. The first event sampled in the LIDAR data, between June 8 and June 10, occurs at a low altitude, with a concentration maximum be-

tween 1000 and 2000 m.a.g.l in both measurements and simulation. During the same period, a strong backscatter signal is also observed in the boundary-layer, corresponding to the maxima of fine particle concentrations in the boundary-layer. This boundary-layer contribution is dominant when there is no significant contribution from dust in the free troposphere, which is the case from June 11 to June 19 (Fig. 7b). Modeled profiles display a structure that is very similar to the observed one. However, it must be pointed out that the modeled dust plume reaches generally higher altitudes, up to about 8 km, than observations.

3.1.3 Speciation

[Fig. 8 about here.]

[Fig. 9 about here.]

For the simulation period, the speciation of the particulate matter in the first model layer (Fig. 8) is shown. For the first model layer, a comparison of PM_{10} speciation has been performed between the model and the measurements, for three categories of aerosols : Total PM_{10}, non-dust PM_{10}, and SSA PM_{10}. It is worth noting at that point that, even though the Lampedusa station is located at an altitude of 45m.a.s.l., we compared the measured concentrations to the concentrations modelled for the first modelled level (0-30m) rather than the second model level (30-70m). We lack small-scale meteorological information to know whether the air masses that arrive at the measurement station come from the first 30 meters above the sea, or from air particles that were already at about the altitude of 45m during their travel above open sea. However, we checked that the modelled concentrations of the various aerosol species above Lampedusa do not change measurably between the first and the second model layer (not shown), so that the results discussed in the present study are not sensitive to that choice.

For total PM_{10} (black lines), the agreement between modelled and measured value is not good, with a large overestimation of aerosol concentration by CHIMERE (the average value for all the times where measured values are available is $41.9\mu gm^{-3}$ in CHIMERE against $18.8\mu gm^{-3}$ in the measurements), with a significant but moderate temporal correlation (correlation coefficient of 0.40). Results for non-dust PM_{10} (blue lines) are much better. Even though the bias in CHIMERE is still strong ($31.7\mu gm^{-3}$ in CHIMERE against $17.6\mu gm^{-3}$ in the measurements), the temporal correlation (R=0.72) is much stronger. The better agreement in non-dust PM_{10} between the model and the measurements permits to conclude that the poor agreement between model and observations for total PM_{10} is in part due to an overestimation of dust concentrations in the first model layer by CHIMERE. Given the vertical structure of the dust layers, that are essentially located in the free troposphere (Fig. 7), this large overestimation of dust concentrations at ground level in Lampedusa may be an indicator of excessive sedimentation (caused either by the sedimentation scheme or by a bias in the size distribution of aerosols), an excessive numerical diffusion in the model compared to reality, or a misrepresentation of the marine boundary layer by the WRF model.

If we now examine the time-series for sea-salt aerosols (Fig. 8, green lines), there is a very good temporal correlation between CHIMERE and the measured values (R=0.90), showing that the evolution of the sea-salt concentration is very well captured by the model. However, a significant bias in modelled values relative to the observations can be observed, due to the presence in the model of a significant background concentration of sea-salt: while the modelled sea-salt concentrations almost always exceed $5\mu gm^{-3}$, the measured values get very close to 0 in some periods. This overestimation of the wind during periods of weak winds can be a factor explaining the excessive backgroung sea-salt concentration. As a summary, simulated PM10 in the boundary layer are overestimated by $25\mu gm^{-3}$ in average in the boundary layer at Lampedusa. This overestimation comes from the mineral dust ($8\mu gm^{-3}$), the sea-spray aerosols ($5\mu gm^{-3}$) and other aerosols ($9.5\mu gm^{-3}$).

Regarding the total aerosol column (Fig. 9), it is generally largely dominated by dust, with dust loads reaching 1-2 gm^{-2} during a sharp peak, and a background level around or below 0.1 gm^{-2}. Therefore, mineral dust is the dominant contributor to the AOD for Lampedusa at least during AOD peaks. At Lampedusa, the other aerosol species contribute to the total aerosol load by at least one order of magnitude less than mineral dust. This is the case of ammonium, sulphates sea-salts and primary anthropogenic particulate matter ($\simeq$0.01-0.1gm^{-2}), while all the other species contribute again one order of magnitude less.

The LIDAR measurements in Fig. 7b,c show that the aerosols in the free troposphere, where dust is dominant (Fig. 9), seem to have a stronger contribution to the total backscatter than aerosols located in the boundary layer, where non-dust aerosols generally dominate (Fig. 8). In that sense, both model and measurements seem to indicate that the dominant contribution to the AOD during the considered period can be attributed to the presence of dust in the free troposphere, at least during periods of AOD peaks. The boundary-layer aerosols such as sea-salt and other species might have a significant contribution to the background AOD values in periods when dust is almost absent from the troposphere above Lampedusa, as it is the case between June 12 and June 18 for example.

Finally, in order to understand the source regions of the aerosols modelled and observed above Lampedusa, we performed a backtrajectory study for two particular times and altitudes (Fig. 10). June 23, 12UTC at 4500 m altitude, is a point selected inside a free tropospheric dust layer (Fig. 7), and June 24, 12UTC at 10 m.a.g.l., corresponds to a zone of strong sea-salt concentration in the marine boundary layer (Fig. 8). Figure 10a shows that the air masses arriving at 4500m above Lampedusa on June, 23 at 12 UTC were all lo-

cated above north-Africa from 72 to 24 hours before their arrival. Over these arid areas where they stayed for several days being caught in the boundary layer every day and detrained every night (Figure 10c), they gained a significant content in mineral dust particles likely due to local emissions. These dust particules are then advected to the vertical of Lampedusa, being in the free troposphere during the last 72 hours of their travel. If we now look at the backtrajectories of the air masses contributing to the strong sea-salt content on June 23 at 12 UTC in the lowest layers (Fig. 8), the backtrajectories (Figure 10b) show that these particles come from the north-west and have travelled 24 hours or more above the western Mediterranean, most of them staying inside the marine boundary layer all along their trajectory (Figure 10d). These trajectories are consistent with the backtrajectories given by Pace et al. (2006) for days with a strong sea-salt content at Lampedusa, and provide a particularly long trajectory of this air mass above water, which favours strong sea-salt content of these air masses (Granier et al. (2004)).

[Fig. 10 about here.]

As a summary of this section, it can be said that :

- The average AOD over most of the simulation domain is simulated correctly by CHIMERE for the considered time period (June 1st to July 15), and compares favorably to MODIS AOD
- The dust plume simulated by CHIMERE over the western Mediterranean from June 13 to June 25 is also captured by MODIS, as well as by the relevant AERONET stations. It has been observed by the LIDAR in Lampedusa at about the same time and altitude as modelled in CHIMERE. The AOD values simulated are realistic, as well as the eastward movement of the plume and its timing at each of the measurement stations.
- At Lampedusa, measurements of the chemical composition of aerosols show that the dust plume has not reached the ground level during the simulation period, which is contrary to the simulation outputs. This overestimation of dust concentration in the boundary layer might be a consequence of excessive numerical diffusion in the model, as discussed in Vuolo et al. (2009).

3.2 Impact of aerosols on photolysis rates at Lampedusa

[Fig. 11 about here.]

[Fig. 12 about here.]

[Table 4 about here.]

3.2.1 Comparison of modelled $J(NO_2)$ to observations

Figure 11a shows the time series of the daily maxima of $J(NO_2)$ in both simulations as well as the $J(NO_2)$ value derived from the Metcon spectrometer measurements at Lampedusa. The measurements take into account only the downward contribution to the actinic flux, while the modelled value also includes the upward flux due to the non-zero albedo of the surface. Since the albedo of the surface in the model has been set to a fixed value of $A = 0.1$ for this simulation, we multiplied the modelled value for $J(NO_2)$ by a correction factor of $1/(1+A)$ in order to obtain a modelled $J(NO_2)$ value plotted in Figure 11a, which is representative of the downward component of the actinic flux only and can therefore be compared directly to the measured values. It is worth noting that the simulation period is centered on the summer solstice, so that the Solar zenith angle at local solar noon only varies from 12.89° on June 6 to 12.07° on June 21. The cosine of that angle (which determines the optical path of incoming solar rays inside the atmosphere) only varies by about 0.3% during the measurement period. This explains the fact that no seasonal trend is visible either in the model or in the measurements, and needs not be taken into account for our study. Similarly, changes in the Sun-Earth distance are very small, and produce a negligible effect on the day-to-day variations in the selected period. Thin clouds were present above the station on June 6, 7, 8, 10, 11, 13, 14, 24 and on July 4 and 5. These days are signalled on Fig. 11a by empty diamonds, while days when no cloud influence exists in the measurements are represented by full diamonds. In the model, cloud cover was present over Lampedusa in daytime only on June 27, June 30 and July 5. However, it is visible on Fig. 11a-b that these clouds were not thick enough to influence the photolytic rates above Lampedusa.

Two observations can be made from Fig. 11a. First, the values of diurnal maxima of $J(NO_2)$ in both simulations are positively biased. This bias is of 12.3% for the simulation without aerosols (NA), and 8.2% in the reference simulation, so that, in average during the simulation period, the direct radiative effect of the aerosol reduced the daily maxima of $J(NO_2)$ by about 4%. The second observation is that the variations of the daily maxima of $J(NO_2)$ in the REF simulation correspond almost exactly to these of the measured data : calculating the linear correlation between these two time series yields a correlation coefficient of 0.92 and a slope of 1.13 (Tab. 4), both representing an excellent correlation between the simulated and measured daily maxima of $J(NO_2)$. This excellent correlation indicates that the variations of $J(NO_2)$ due to the optical effect of aerosols are very well represented in this simulation. Comparison between Figs. 11a and 6a shows that this effect is mostly substantial only when the AOD reaches or exceeds values arount 0.2. This result clearly shows that taking into account the optical effect of aerosols gives a strong added value in the capacity of a model to reproduce day-to-day variations in the photolytic rates.

[Fig. 13 about here.]

It is also interesting to examine the representation of the diurnal cycles of $J(O^1D)$ and $J(NO_2)$ in CHIMERE for both clear days and days with a moderate AOD. For that purpose, based on AOD value and data availability, we selected June 18 as a representative clear-sky day, and June 23 as a day representative of a moderate dust outbreak. Measured AOD value is about 0.1 for June 18, and modelled AOD about 0.12 for the same day, while for June 23, measured AOD is about 0.35 and modelled AOD is about 0.45 in average. Figure 12a shows the simulated and observed diurnal cycle of $J(NO_2)$ for these two days. For June 18 (Fig. 12a), it can be seen that the values in the morning and the evening are simulated very realistically by both simulations, while both simulations overestimate $J(NO_2)$ around local noon. For June 23, the time evolutions of measured $J(NO_2)$ have variations from an hour to another. The modelled $J(NO_2)$ values in the REF simulations does not have such variations, suggesting that the spatial resolution of the CHIMERE model and the smoothing of dust plumes by numerical diffusion lead CHIMERE to miss some fine-scale spatial structures of the plume. Despite this lack of rapid variations, the REF simulation does much better than the NA simulation in representing $J(NO_2)$ for that day. The simulated values for the REF simulations are either stronger or weaker than the measured values, depending on the hour. The systematic overestimation of $J(NO_2)$ by the model around local noon is still present for that day, but the model bias is much weaker in the REF simulation than in the NA simulation.

A scatter plot of modelled vs. observed $J(NO_2)$ values (Fig. 13a) confirms that the relationship between observed and modelled $J(NO_2)$ values is excellent for both simulations, even though discrepancies between observed and simulated values are stronger in the NA simulation than in the REF simulation. The correlation coefficient (Table 4) is higher in the REF simulation (0.993) than in the NA simulation (0.987), being excellent in both cases. Since $J(NO_2)$ is essentially a function of the solar zenith angle, these very high correlation coefficients primarily show that the dependence of $J(NO_2)$ on the solar zenith angle is represented very well by the CHIMERE model.

3.2.2 Comparison of modelled $J(O^1D)$ to observations

Figure 11b shows the time series of the daily maxima of $J(O^1D)$ for both the REF and the NA simulation as well as in the measurements when available.

Comparison of the daily maxima between the REF and the NA simulation shows that the effect of the aerosols above Lampedusa on the $J(O^1D)$ for that period reduces the daily maximum of $J(O^1D)$ by 3% to 20%, depending on the AOD (Fig. 11b). The minimal value of the daily maximum $J(O^1D)$ is reached on June 6th, both in the REF simulation and in the observations, possibly due to a sharp peak in AOD for that day (Fig. 6a). The peak in modelled dust load and in simulated and observed AOD between June 20 and June 25 (Fig. 6a) generates another period of strong impact of aerosols on $J(O^1D)$, both in the model and in the observations.

From a statistical point of view (Table 4), the NA simulation, without the direct effect of the aerosols, has no ability to reproduce the day-to-day variations of $J(O^1D)$ (R=0.09, p-value=0.65). On the contrary, the REF simulation, including the aerosol direct effect, has a correlation coefficient of 0.46 to the observations, and a p-value of 0.02 that gives good confidence in this result despite the reduced size of the sample (26 points). This shows that taking into account the direct optical effect of the aerosols permits to CHIMERE to better represent the measured day-to-day variations of $J(O^1D)$.

The correlation coefficient of daily maxima in $J(O^1D)$ between the REF simulation and the observed values is only 0.46, much lower than the value of 0.92 obtained for $J(NO_2)$ correlation. This lower value can be explained by the fact that, even when clouds are not present, $J(O^1D)$ is influenced by other factors than the AOD, and first of all by the total ozone column. From that point of view, the period for which measurements of $J(O^1D)$ are available, from June 5 to July 5, can be separated into two periods according to the total ozone column (Fig. 3). In the first half of June, until June 13, the values of ozone column oscillate around 340 DU, in the second half of June and the beginning of July, it oscillates around 310 DU. This transition is reflected on Fig. 11b by stronger $J(O^1D)$ value after June 14 than before June 13, corresponding to a thinner ozone column. This large variation of the measured $J(O^1D)$ values is not captured by the model, which uses prescribed values for stratospheric ozone. The dependence on temperature is also a possible explanation of the different variations between the observed and modelled $J(O^1D)$ values, since the modelled temperature values in the boundary layer are not representative of the local temperature at Lampedusa (Fig. 1). On the contrary, $J(NO_2)$ has only a marginal dependence on the total ozone column, which explains the very high correlation coefficient obtained between the observed and modelled values (0.92). Therefore, the moderate correlation of daily maxima of $J(O^1D)$ (0.46) between modelled and observed values must not be blamed on a bad representation of aerosols in the model, but rather on the absence of variations of the stratospheric ozone column in the model.

As for $J(NO_2)$, we examine the diurnal cycles for June 18 and June 23, considered as representative of clear days and days with a strong AOD, respectively. If we first look at the clear-sky measured and modelled diurnal cycles, (Figs. 12c), as could be expected, we see that the simulated $J(O^1D)$ values in the NA simulation are barely different from those in the REF simulation, revealing a very small impact of the AOD on photolytic rates for that day. Comparison of simulated $J(O^1D)$ to the observed values (Fig. 12c) shows that both simulation simulate quite realistically the observed $J(O^1D)$ for that day, with a slight underestimation of $J(O^1D)$ by the model, particularly around local noon. The

general shape of the diurnal cycle of $J(O^1D)$ is captured very well by the model. For June 23, on the contrary, the REF and the NA simulations are very different due to the strong dust column. Compared to June 18, the reduction in $J(O^1D)$ is strong for both the REF simulation (11% at local noon) and the measured values (7%). It is worth noting that the weaker reduction of the measured $J(O^1D)$ compared to the simulated $J(O^1D)$ between June 18 and June 23 can also be attributed to a compensation between the optical effect of aerosols, tending to reduce observe $J(O^1D)$, and the thinning ozone column between these two dates (Fig. 3), tending to compensate the effect of dust. This compensation effect between the effects of changes in AOD and in total ozone column on surface UV irradiance, and thus also on $J(O^1D)$, has been discussed by di Sarra et al. (2002), who have shown that during spring and summer at Lampedusa, the synoptic conditions leading to dust transport also induce thinner ozone colums.

Figure 13a confirms that the representation of the diurnal cycle of $J(O^1D)$ at Lampedusa by the Fast-JX module within CHIMERE is very satisfactory. The linear correlation coefficient between the observed and modelled value for the REF simulation is of 0.981, slightly stronger than the value of 0.972 obtained for the NA simulation (Table 4). The high values of these correlation coefficients for both simulations confirm that the general shape of the diurnal cycle of $J(O^1D)$ is captured very well by both simulations, confirming that the dependence of $J(O^1D)$ on the solar zenith angle is represented correctly by the CHIMERE model. The average of the 610 valid data points, representative of average daytime $J(O^1D)$ during the simulation, is lower by 5.8% when compared to the observations, while the NA simulation has a positive bias of 2.3%.

3.2.3 Dependence of $J(O^1D)$ and $J(NO_2)$ on the AOD at fixed zenith angle

Finally, in order to evaluate directly the impact of the aerosols on $J(O^1D)$ and $J(NO_2)$, as in Gerasopoulos et al. (2012) and Casasanta et al. (2011), we produced scatter plots representing the modelled photolysis rates as a function of the modelled AOD at 400nm for clear sky conditions and for a fixed zenith angle (Fig. 14). These scatter plots have been produced by selecting, for all the model points located at about the same latitude as Lampedusa (35.5°N±3°), the times when no clouds are present in the model, and for which the SZA corresponds to the target SZA (30° and 60°) within a tolerance margin of ±1°. As discussed above, the modelled photolysis rates have been muntiplied by $\frac{1}{1+A}$ where A is the albedo, fixed at 0.1 in the model, in order to permit the comparison of the model outputs with measurements that take into account only the downward actinic flux. The size of the dataset for modelled values is very large (12637 points for panels a and c ; 12916 points for panels b and d) and describe an AOD range from 0 to values that largely exceed unity. The regression lines provided by Gerasopoulos et al. (2012) for $J(NO_2)$ and by Casasanta et al. (2011) have also been superposed to the scatter plots displayed for comparison. It is worth noting at this point that, during our simulation period, no significant AOD peaks have been simulated due to non-dust aerosols, so that the scatter plot obtained in the REF simulation (Fig. 14b) shall be compared to the red regression line given by Gerasopoulos et al. (2012) for cases when dust predominates rather than to the blue regression line given for cases when non-dust aerosols predominate.

Regarding $J(NO_2)$, Fig. 14b reproduces the linear relationships given in Gerasopoulos et al. (2012) (their Fig. 6) for $J(NO_2)$ vs AOD at 60° zenith angle. The red line concerns the relationship they establish when the AOD is predominantly due to dust, and the blue line for AOD predominantly due to other aerosols. From the location of our modelled points relative to these linear relationships established from measurement data, it can be said that the quasi-linear dependence between $J(NO_2)$ and the AOD for a fixed zenith angle is reproduced very well by the Fast-JX module in CHIMERE. It can also be inferred from this figure that the relationship between $J(NO_2)$ and the AOD proposed by Gerasopoulos et al. (2012) for the cases when dust aerosols predominates seems to be valid much beyond the AOD range observed in their dataset, which only covered AOD values up to 0.65, against 1.9 in Fig. 14b. For a SZA value of 30° (Fig. 14a), the dependence of $J(NO_2)$ on the AOD is also consistent with the results of Gerasopoulos et al. (2012): the figure 10 of these authors indicates an effect between 10 and 15% on $J(NO_2)$ for an AOD value of 0.7, very similar to what we observe on Fig. 14a. At that point, it is worth going back to Table 4. Analysis of the correlation (0.92) and slope (1.13) of the linear regression between observed and simulated daily maximal values, representative of SZA values ranging between 12 and 13°, shows that, for the very small SZA values corresponding to solar noon conditions at Lampedusa, the effect of the aerosol optical depth on $J(NO_2)$ at very small SZA values is represented realistically as well.

Regarding $J(O^1D)$, panels c and d of Fig. 14 present the scatter plots of $J(O^1D)$ in this study against AOD for cloud-free condition at a SZA of 30° and 60° respectively. The correlation lines provided by Casasanta et al. (2011) (their Table 2) are also reported on these panels, along with the maximal and minimal hypothesis obtained by applying to the slope and intercept values an uncertainty margin of $\pm 2.5\sigma$, where the uncertainty value σ is provided by these authors. We chose to apply the relationships obtained by Casasanta et al. (2011) for a total ozone column of 280-290DU, which is the closest values to the modelled ozone columns in the present study. At 30°, the simulated relationship between AOD and $J(O^1D)$ in this study is within the uncertainty range of the linear relationships given by Casasanta et al. (2011), with a large spread in modelled data, maybe due to the very different surface temperatures that can be observed

across the domain even at a constant latitude. The reduction of $J(\mathrm{O^1D})$ by a unit AOD in the simulated values is of about 25%, smaller than the value of 38% that can be obtained from the results of Casasanta et al. (2011) (their Table 2). This seems to indicate that the effect of the AOD on $J(\mathrm{O^1D})$ might be underestimated by the Fast-JX algorithm within the CHIMERE model, which is even more the case for 60° SZA (Fig. 14d), for which the modelled scatter plot is clearly out of the uncertainty range obtained by appling a $\pm 2.5\sigma$ uncertainty margin to the slope given by these authors. Therefore, it seems that the effect of the AOD on $J(\mathrm{O^1D})$ in CHIMERE might be underestimated, particularly for the high SZA values.

[Fig. 14 about here.]

3.3 Impact of the aerosols on the concentration of trace gases

Time series of the simulated ozone concentration is shown in Fig. 15a for the Lampedusa station, and compared to measurements. Figure 15a shows that the agreement between model and measurements at Lampedusa for the simulation period is rather satisfying. The ozone concentrations evolve between 30 ppb and 70 ppb during this period, with a diurnal cycle of about 10 ppb which is captured by the model. The model is also able to capture the low ozone period between June 20 and July 5, and the higher ozone concentrations before and after that period. Fig. 15b shows the net effect of the AOD on ozone concentration at Lampedusa showing that the effect of the AOD on ozone concentration is almost always negative at that location, reaching $-2\mathrm{ppb}$ during the dust outbreak of June 20-25 above Lampedusa, for a simulated AOD about 0.4.

[Fig. 15 about here.]

[Fig. 16 about here.]

Figure 16 shows the spatial distribution of the aerosol effects on photochemistry averaged over the whole simulated period. The effect of the AOD on both $J(\mathrm{O^1D})$ and $J(\mathrm{NO_2})$ ranges between a few percents for areas in the northern parts of the domain that present a small average AOD, and about 20% in the areas that are close to the sources of dust in Africa or downwind of them over the tropical Atlantic ocean. Over the whole domain, as could be expected, the average effect of aerosols is to reduce both $J(\mathrm{O^1D})$ and $J(\mathrm{NO_2})$, affecting both rates in a very similar proportion. Regarding the net average effect of the AOD on ozone concentration, the picture is very contrasted (Fig. 16c). Over the Mediterranean Sea, the northeast Atlantic and continental Europe, as well as parts of equatorial Africa, the effect of the reduction in photolytic rates leads to a net average reduction in ozone concentrations, as could be seen for Lampedusa in Fig. 15. This reduction locally reaches $1\mathrm{ppb}$ over the Mediterranean basin, as well as in areas of equatorial Africa. On the contrary, over the Saharan desert as well as over the tropical Atlantic below the dust plume, ozone concentration seems to be increased by this reduction in the photochemical reaction rates. Comparison of Fig. 16c with the NO_x emissions as shown on Fig. 2 shows that the effect of the reduction of the photolysis rates by aerosol screening depends on the presence of important NO_x emissions: in areas close to significant sources of NO_x such as Continental Europe, coastal North-Africa, Turkey and the Middle East, Nigeria, and the shipping routes in the Mediterranean and the Red Sea, the effect of aerosol screening is to reduce ozone concentrations, by reducing its photochemical production through the photodissociation of NO_2, due to the decrease of $J(\mathrm{NO_2})$. On the contrary, over remote areas such as the Saharan desert and the tropical Atlantic, the effect of aerosol screening is to increase ozone concentrations, most likely by reducing photochemical dissociation of ozone. This confirms the findings of Bian et al. (2003b) in a global scale CTM: these authors also observed in their model that the sign of the effect of AOD on ozone concentrations changes according to the photochemical regime, due to the competition effect between reduced ozone formation due to the reduction of $J(\mathrm{NO_2})$, and reduced ozone destruction due to the reduction of $J(\mathrm{O^1D})$, yielding, according to the photochemical regime, to a positive, negative or neutral effect of AOD on ozone concentration.

3.4 Sensitivity to a bias in total ozone column

The total ozone column in the model is biased towards low values when compared to observations (Fig. 3). In order to measure the impact of this underestimation on the ability of the CHIMERE model to accurately simulate the value of $J(\mathrm{O^1D})$ in the troposphere, it is interesting to examine at this point the outputs of the *O3+* simulation performed enhancing the ozone concentrations used for radiative calculations throughout the atmosphere, thereby compensating the bias on ozone column visible on Fig. 3. The effect of this increase of 18% of the total ozone column is to reduce the modelled $J(\mathrm{O^1D})$ by about 20% in Lampedusa (Fig. 11) as well as in the rest of the domain (not shown), with a stronger reduction in the northern part of the domain and a weaker reduction in the south. As the bias in $J(\mathrm{O^1D})$ was weak in the REF run (Fig. 11), the $J(\mathrm{O^1D})$ photolytic rates in the *O3+* simulation have a strong negative bias of about 20% compared to the measured values. The temporal variations of $J(\mathrm{O^1D})$ are not changed very much by this debiasing of ozone column (Fig. 11).

As expected (Fuglestvedt et al., 1994), $J(\mathrm{NO_2})$ values show a very small sensitivity to this debiasing of the ozone column. The increase of 18% in the model ozone column results in a reduction by about 0.3% of the average $J(\mathrm{NO_2})$ over the entire domain.

The effect of the modification of the ozone column on ozone concentrations is significant (Fig. 17), with an increase

of up to 4 ppb of the ozone concentrations over remote areas such as the Saharan area and the eastern Mediterranean, and a weaker increase of ozone concentrations aver continental Europe. This increase of ozone concentrations can be attributed to the reduction of ozone photolysis due to the increased ozone column and the reduced value of $J(O^1D)$. Interestingly, this reduction of $J(O^1D)$ has the contrary effect over the North Sea, resulting in slightly increased ozone concentrations (about 1 ppb). Generally speaking, it is visible in Fig. 17 that in regions having large anthropogenic emissions such as northern Europe, the Po valley and regions with intense shipping in the Mediterranean, Atlantic, North Sea and Baltic Sea, the effect of the reduced $J(O^1D)$ on ozone concentrations is weak, while it is much stronger in areas far away from the main emissions zones.

The fact that taking into account a debiased ozone column creates a negative bias on $J(O^1D)$ suggest that, from a modelling point of view, using Fast-JX version 7.0b as it is provided, even with the fact that the ozone climatology delivered along with the model seems to be biased, gives better results in terms of photolytic rates than when the total ozone column is debiased. This counterintuitive result indicates that, from a practical point of view, it is better to use Fast-JX 7.0b with the stratospheric ozone column as it is provided, because the $J(O^1D)$ values calculated with a more realistic ozone column are negatively biased. This highlights the conception of Fast-JX as a tool designed to perform fast and accurate calculations of the photolytic rates within a CTM, rather than a tool made to solve exactly every aspect of the radiative transfers in the atmosphere.

[Fig. 17 about here.]

4 Conclusions

Three simulations of the atmospheric composition have been performed for the period covering June 6 - July 15, 2013, for a large domain including the Mediterranean Sea as well as the surrounding continents and the northeastern part of the Atlantic Ocean. The reference simulation (REF) is the same as described in Menut et al. (2015), while the second simulation is a sensitivity simulation performed without taking into account the optical effect of aerosols on photochemistry (NA simulation). Comparison with MODIS satellite data as well as with AERONET and MFRSR observations shows that the reference simulation reproduces realistic levels of AOD over most of the simulation domain, including the main study area in Lampedusa: in the case of Lampedusa, the correlation coefficient between simulated and observed AOD at 400 nm is strong (0.8), with an average positive bias of 0.04 in the simulated AOD (19.08% of the average observed value). These correlation and bias of the simulated vs observed values vary greatly depending on the measurement stations. For stations in north Africa or around the Mediterranean, the bias is generally moderate (-35% to +17,9% in the ten considered stations) and the correlation coefficients vary from -0.14 to 0.79. For the two stations that were considered in northern Europe (Palaiseau, France, and Mainz, Germany), the negative bias in the simulated values is strong (-61.7% and -45.3% respectively), with very weak correlation coefficient. It is also of interest to note that the peak AOD values at the Lampedusa and Palma de Mallorca stations tend to be overestimated by up to 50% by the CHIMERE model during the simulation period.

Regarding the speciation of the aerosols close to the ground at Lampedusa, these simulations show a good capability to represent the non-dust PM_{10} concentrations at ground level and their variations, mainly due to sea-salt aerosols. On the contrary, the dust concentrations close to the ground level are too strong in the model compared to the observations, possibly indicating an excess of vertical diffusion and/or sedimentation in the model. A third simulation (O3+) has been performed in order to locally remove the bias in the total ozone column in the model compared to observations above Lampedusa.

Regarding the photolytic rates, it is shown that both the REF and NA simulations simulate the photolytic rates $J(O^1D)$ and $J(NO_2)$ in a satisfactory way for Lampedusa, when compared to in-situ measurements. The REF simulation is biased by 5.8% towards an underestimation of the observed $J(O^1D)$ value, and the NA simulation is biased by about 2.3% towards an overestimation. However, two large uncertainty factors affect the modelled $J(O^1D)$ values: the climatology of stratospheric ozone that has been used for this study did not fit the observed total ozone column, and the temperature in the model was negatively biased as well. Regarding the representation of $J(NO_2)$, the NA simulation exhibits an overestimation of 12.3% in $J(NO_2)$ compared to observations, which is largely corrected by the inclusion of the aerosols, as reflected by the much smaller bias in the REF simulation (4.8%). If we turn to the variations of $J(NO_2)$ and $J(O^1D)$ with time, the correlation coefficient between hourly simulated and measured values is excellent for both simulations, always in excess of 0.97, reflecting the fact that the diurnal cycle of $J(O^1D)$ and $J(NO_2)$ is represented very realistically by the Fast-JX module within the CHIMERE model. If we remove the impact of the diurnal cycle by comparing the daily maxima of $J(O^1D)$ and $J(NO_2)$ in both simulations to measurements, it becomes clear that the day-to-day variability of $J(O^1D)$ is represented much better in the REF simulation than in the NA simulation. While the simulation without effect of the aerosols is not able to reproduce any of the observed day-to-day variations in $J(O^1D)$, the daily maxima of $J(O^1D)$ REF simulation are significantly correlated to the observed values. Therefore, despite the strong dependence of $J(O^1D)$ on the total ozone column, it is safe to state that the inclusion of the optical effect of aerosols improves the representation of the evolution of $J(O^1D)$ in the CHIMERE model. Regarding $J(NO_2)$, the

added value of including the aerosol effects is more spectacular since $J(NO_2)$ has no strong dependence on the total ozone column (Fuglestvedt et al., 1994). The REF simulation captures almost exactly the day-to-day variations of $J(NO_2)$ (R=0.92), while the NA simulation does not capture any of these variations, showing that, in the near-absence of clouds, representing correctly the effect of the aerosols is a necessary and sufficient condition to represent the day-to-day variations of $J(NO_2)$.

The relationship between $J(O^1D)$ and the AOD at a constant zenith angle, as well as for $J(NO_2)$ in CHIMERE has been compared to the results of Gerasopoulos et al. (2012) for $J(NO_2)$ and Casasanta et al. (2011) for $J(O^1D)$. This comparison shows that the dependence of $J(NO_2)$ on the AOD as represented by CHIMERE is very similar to the observational results of Gerasopoulos et al. (2012). Our model results indicate a reduction of $J(NO_2)$ by a unit AOD of about 20% for a SZA value of 30°, and 35% for a SZA value of 30°. Regarding $J(O^1D)$, the comparison of our model results with the results of Casasanta et al. (2011), obtained from *in situ* measurements, seems to indicate that the effect of the aerosols on $J(O^1D)$ is underestimated in CHIMERE, particularly for high SZA values (60°). However, from a modelling point of view, this caveat is not critical since photochemistry is not very active when the SZA is so high.

Finally, regarding the optical impact of the aerosols on the ozone concentration through the modulation of the photolytic rates, comparison between the REF simulation and the NA simulation shows that, above Lampedusa, the optical effect of the aerosols reduced the ozone concentration by up to 2 ppb during the dust transport episode that occured between June 20-25 above Lampedusa. This result is consistent with the results of Bian et al. (2003b), and as these authors we interpret this reduction as an effect of lower photochemical ozone production in Lampedusa and the surrounding marine and continental areas due to reduced photolysis rates. Over other parts of the simulation domain, such as the Saharan desert, the impact of optical screening by mineral dust is, on the contrary, to increase the ozone concentration. This twofold effect of the optical screening of the incoming shortwave radiation by the aerosols might be explained by the balance between the reduction of $J(NO_2)$, which tends to reduce ozone production particularly in zones under anthropogenic influence, and the reduction of $J(O^1D)$, which tends to reduce ozone destruction.

From a modelling point of view, the main conclusion of this study is that including an online representation of the photolysis rates taking into account the real-time simulated aerosol concentrations with a realistic model for radiative transfers such as Fast-JX permits a much better representation of photolytic rates compared to measurements. This is particularly true for $J(NO_2)$: the representation of $J(O^1D)$ is much more complex, particularly due to the effect of the variations in the total ozone column, which are superposed to the variations due to the AOD. The impact on ozone concentrations in the present study is moderate (a few ppb), which might be due to the relatively coarse model resolution. The impact of modulation of photolytic rates by the AOD may very well be more important in urban conditions where important aerosol loads from natural and anthropogenic sources occur at the same time and place as massive emissions of nitrogen oxides.

Acknowledgement

We thank the ChArMEx program (sponsored by CNRS-INSU, ADEME, Météo-France and CEA) as well as the ADRIMED program (sponsored by ANR) for permitting the collection of the relevant field data, the principal investigators of the three AERONET stations that have been used in this study: Daniela Meloni for Lampedusa, Diouri Mohammed and Djamaleddine Chabane for Oujda, Juan Ramon Moreta Gonzalez for Palma de Mallorca. Measurements at Lampedusa during ChArMEx were partly supported by the Italian Ministry for University and Research through the NextData and Ritmare projects. The contributions by Lorenzo De Silvestri are gratefully acknowledged. The authors also wish to thank the Editor for his careful editorial and scientific review of the initial manuscript, as well as the three anonymous Reviewers who largely helped to improve this study.

References

Alfaro, S. C. and Gomes, L.: Modeling mineral aerosol production by wind erosion: Emission intensities and aerosol size distributions in source areas, J. of Geophys. Res., 106, 18 075–18 084, doi:10.1029/2000JD900339, http://dx.doi.org/10.1029/2000JD900339, 2001.

Bessagnet, B., Hodzic, A., Vautard, R., Beekmann, M., Cheinet, S., Honoré, C., Liousse, C., and Rouil, L.: Aerosol modeling with CHIMERE: preliminary evaluation at the continental scale, Atmos. Environ., 38, 2803–2817, 2004.

Bian, H., , and Prather, M.: Fast-J2: accurate simulation of stratospheric photolysis in global chemical models, J. Atmos. Chem., 41, 281–296, 2002.

Bian, H., , and Zender, C. S.: Mineral dust and global tropospheric chemistry: relative roles of photolysis and heterogeneous uptake, J. Geophys. Res., 108, doi:10.1029/2002JD003143, 2003a.

Bian, H., Prather, M. J., and Takemura, T.: Tropospheric aerosol impacts on trace gas budgets through photolysis, J. Geophys. Res., 108, doi:10.1029/2002JD002743, 2003b.

Bowen, H. J. M.: Environmental Chemistry of the Elements, Academic Press, London, 1979.

Casasanta, G., di Sarra, A., Meloni, D., Monteleone, F., Pace, G., Piacentino, S., and Sferlazzo, D.: Large aerosol effects on ozone photolysis in the Mediterranean, Atmos. Environ., 45, 3937–3943, 2011.

Chen, F. and Dudhia, J.: Coupling an Advanced Land SurfaceâĂŞHydrology Model with the Penn StateâĂŞNCAR MM5 Modeling System. Part I: Model Implementation and Sensitivity, Mon. Weath. Rev., 129, 569âĂŞ585, 2001.

Davidson, J. A., Cantrell, C. A., Mcdaniel, A. H., Shetter, R. E., Madronich, S., , and Calvert, J. G.: Visible-ultraviolet absorption sross sections for NO2 as a function of temperature, J. Geophys. Res., 93, 7105–7112, 1988.

Di Iorio, T., di Sarra, A., Sferlazzo, D. M., Cacciani, M., Meloni, D., Monteleone, F., Fuà, D., and Fiocco, G.: Seasonal evolution of the tropospheric aerosol vertical profile in the central Mediterranean and role of desert dust, J. Geophys. Res., 114, D02 201, doi:10.1029/2008JD010593, 2009.

di Sarra, A., Cacciani, M., Chamard, P., Cornwall, C., DeLuisi, J. J., Di Iorio, T., Disterhoft, P., Fiocco, G., Fuà, D., and Monteleone, F.: Effects of desert dust and ozone on the ultraviolet irradiance at the Mediterranean island of Lampedusa during PAUR II, J. Geophys. Res., 107, PAU 2–1 – PAU 2–14, doi: 10.1029/2000JD000139, 2002.

di Sarra, A., Sferlazzo, D., Meloni, D., Anello, F., Bommarito, C., Corradini, S., and Di Iorio, T.: Empirical correction of multifilter rotating shadowband radiometer (MFRSR) aerosol optical depths for the aerosol forward scattering and development of a long-term integrated MFRSR-Cimel dataset at Lampedusa., Appl. Opt., doi:10.1364/AO.54.002725, 2015.

Diaz, J., Exposito, F., Torres, C., Herrera, F., Prospero, J., and Romero, M.: Radiative properties of aerosols in Saharan dust outbreaks using ground-based and satellite data: Applications to radiative forcing, J. Geophys. Res., 106, 18 403–18 416, 2001.

Dickerson, R. R., Stedman, D. H., and Delany, A. C.: Direct measurements of ozone and nitrogen dioxide photolysis rates in the troposphere, Journal of Geophysical Research: Oceans, 87, 4933–4946, doi:10.1029/JC087iC07p04933, http://dx.doi.org/10.1029/JC087iC07p04933, 1982.

Favez, O., Cachier, H., Sciare, J., Alfaro, S. C., El-Araby, T., Harhash, M. A., and Abdelwahab, M. M.: Seasonality of major aerosol species and their transformations in Cairo megacity, Atmos. Environ., 42, 1503–1516, 2008.

Fuglestvedt, J. S., Jonson, J. E., and Isaksen, I. S. A.: Effects of reductions in stratospheric ozone on tropospheric chemistry through change in photolysis rates, Tellus, 46 B, 172–192, 1994.

Gardner, E., Sperry, P. D., and Calvert, J. C.: Primary quantum yields of NO2 photodissociation, J. Geophys. Res., 92, 6642–6652, 1987.

Gerasopoulos, E., Kazadzis, S., Vrekoussis, M., Kouvarakis, G., Liakakou, E., Kouremeti, N., Giannadaki, D., Kanadikou, M., Bohn, B., and Mihalopoulos, N.: Factors affecting O_3 and NO_2 photolysis frequencies measured in the eastern Mediterranean during the five-year period 2002-2006, J. Geophys. Res., p. D22305, doi:10.1029/2012JD017622, 2012.

Ginoux, P., Chin, M., Tegen, I., Prospero, J. M., Holben, B., Dubovik, O., and Lin, S. J.: Sources and distributions of dust aerosols simulated with the GOCART model, J. of Geophys. Res., 106, 20 255–20 273, 2001.

Granier, C., Artaxo, P., and Reeves, C. E., eds.: Emissions of Atmospheric trace Compounds, chap. Sea-salt aerosol source functions and emissions, pp. 333–359, Springer, doi:10.1007/978-1-4020-2167-1_9, 2004.

Grell, G. and Devenyi, D.: A generalized approach to parameterizing convection combining ensemble and data assimilation techniques., Geophys. Res. Lett., 29, doi:10.1029/2002GL015311, 2002.

Guinot, B., Cachier, H., and Oikonomou, K.: Geochemical perspectives from a new aerosol chemical mass closure, Atmos. Chem. Phys., 7, 1657–1670, doi:doi:10.5194/acp-7-1657-2007, 2007.

Hauglustaine, D. A., Hourdin, F., Jourdain, L., Filiberti, M.-A., Walters, S., Lamarque, J.-F., and Holland, E. A.: Interactive chemistry in the Laboratoire de Meteorologie Dynamique general circulation model: Description and background tropospheric chemistry evaluation, J. Geophys. Res., 109, doi:10.1029/2003JD003,957, 2004.

Herich, H., Tritscher, T., Wiacek, A., Gysel, M., Weingartner, E., Lohmann, U., Baltensperger, U., and Cziczo, D. J.: Water uptake of clay and desert dust aerosol particles at sub- and supersaturated water vapor conditions, Phys. Chem. Chem. Phys., 11, 7804–7809, doi:10.1039/B901585J, http://dx.doi.org/10.1039/B901585J, 2009.

Hong, S. Y., Noh, Y., and Dudhia, J.: A new vertical diffusion package with an explicit treatment of entrainment processes, Mon. Weath. Rev., 139, 2318–2341, 2006.

Kaufman, Y., Tanré, D., Dubovik, O., Karnieli, A., and Remer, L. A.: Absorption of sunlight by dust as inferred from satellite and ground-based remote sensing, Geophys. Res. Lett., 28, 1479–1482, 2001.

Keene, W. C., Sander, R., Pszenny, A. A. P., Vogt, R., Crutzen, P. J., and Galloway, J. N.: Aerosol pH in the marine boundary layer: a review and model evaluation, J. Aerosol Sci., 29, 339–356, 1998.

Kinne, S., Lohmann, U., Feichter, J., Schulz, M., Timmreck, C., Ghan, S., Easter, R., Chin, M., Ginoux, P., Takemura, T., Tegen, I., Koch, D., Herzog, M., Penner, J., Pitari, G., Holben, B., Eck, T., Smirnov, A., Dubovik, O., Slutsker, I., Tanre, D., Torres, O., Mishchenko, M., Geogdzhayev, I., Chu, D. A., and Kaufman, Y.: Monthly averages of aerosol properties: A global comparison among models, satellite data, and AERONET ground data, J. Geophys. Res., 108, n/a–n/a, doi:10.1029/2001JD001253, http://dx.doi.org/10.1029/2001JD001253, 2003.

Kishcha, P., Nickovic, S., Starobinets, B., di Sarra, A., Udisti, R., Becagli, S., Sferlazzo, D., Bommarito, C., and Alpert, P.: Sea-salt aerosol forecasts compared with daily measurements at the island of Lampedusa (Central Mediterranean), Atmos. Res., 100, 28–35, 2011.

Levy II, H., Horowitz, L. W., Schwartzkopf, M. D., Ming, Y., Jolaz, J.-C., Naik, V., and Ramaswamy, V.: The roles of aerosol direct and indirect effects in past and future climate change, J. Geophys. Res. Atmospheres, 118, 4521–4532, doi:10.1002/jgrd.50192, 2013.

Marconi, M., Sferlazzo, D. M., Becagli, S., Bommarito, C., Calzolai, G., Chiari, M., di Sarra, A., Ghedini, C., Gómez-Amo, J. L., Lucarelli, F., Meloni, D., Monteleone, F., Nava, S., Pace, G., Piacentino, S., Rugi, F., Severi, M., Traversi, R., and Udisti, R.: Saharan dust aerosol over the central Mediterranean Sea: PM10 chemical composition and concentration versus optical columnar measurements, Atmos. Chem. Phys., 14, 2039–2054, doi: 10.5194/acp-14-2039-2014, 2014.

Marticorena, B. and Bergametti, G.: Modelling the atmospheric dust cycle: 1-Design a soil-derived dust emissions scheme, J. Geophys. Res., 100, 16 415–16 430, 1995.

McPeters, R., Labow, G., and Johnson, B. J.: A satellite-derived ozone climatology for ballonsonde estimation of total column ozone, J. Geophys. Res., 102, 8875–8885, 1997.

Meloni, D., di Sarra, A., herman, J. R., Monteleone, F., and Piacentino, S.: Comparison of ground-based and TOMS erythemal

UV doses at the island of Lampedusa in the period 1998-2003, J. Geophys. Res., 110, D01 202, doi:10.1029/2004JD005283, 2005.

Menut, L., Bessagnet, B., Khvorostyanov, D., Beekmann, M., Blond, N., Colette, A., Coll, I., Curci, G., Foret, G., Hodzic, A., Mailler, S., Meleux, F., Monge, J.-L., Pison, I., Siour, G., Turquety, S., Valari, M., Vautard, R., and Vivanco, M. G.: CHIMERE 2013: a model for regional atmospheric composition modelling, Geoscientific Model Development, 6, 981–1028, doi:10.5194/gmd-6-981-2013, http://www.geosci-model-dev.net/6/981/2013/, 2013.

Menut, L., Mailler, S., Siour, G., Bessagnet, B., Turquety, S., Rea, G., Briant, R., Mallet, M., Sciare, J., and Formenti, P.: Analysis of the atmospheric composition during the summer 2013 over the Mediterranean area using the CHARMEX measurements and the CHIMERE model, Atmos. Chem. Phys. Discuss, submitted, 2015.

Michalakes, J., Dudhia, J., Gill, D., Henderson, T., Klemp, J., Skamarock, W., and Wang, W.: The Weather Research and Forecast Model: Software Architecture and Performance, Proceedings of the Eleventh ECMWF Workshop on the Use of High Performance Computing in Meteorology. 25 - 29 October 2004, Reading, U.K., Ed. George Mozdzynski, 2004.

Mischenko, M., Travis, L. D., and Lacis, A. A.: Scattering, absorption and emission of light by small particles, Cambridge University Press, Cambridge, 2002.

Nenes, A., Pilinis, C., and Pandis, S.: ISORROPIA: A new thermodynamic model for inorganic multicomponent atmospheric aerosols, Aquatic Geochem., 4, 123–152, 1998.

Pace, G., di Sarra, A., Meloni, D., Piacentino, S., and Chamard, P.: Aerosol optical properties at Lampedusa (central Mediterranean). 1. Influence of transport and identification of different aerosol types, Atmos. Chem. Phys, 6, 697–713, 2006.

Putaud, J. P., Van Dingenen, R., Dell'Acqua, A., Raes, F., Matta, E., Decesari, S., Facchii, M. C., and Fuzzi, S.: Size-segregated aerosol mass closure and chemical composition in Monte Cimone (I) during MINATROC, Atmos. Chem. Phys., 4, 889–902, doi:doi:10.5194/acp-4-889-2004, 2004.

Real, E. and Sartelet, K.: Modeling of photolysis rates over Europe: impact on chemical gaseous species and aerosols, Atmos. Chem. Phys, 11, 1711–1727, doi:10.5194/acp-11-1711-2011, 2011.

Remer, L. A., Kleidman, R. G., Levy, R. C., Kaufman, Y. J., Tanré, D., Mattoo, S., Vanderlei martins, J., Ichoku, C., Koren, I., Yu, H., and Holben, B. N.: Global aerosol climatology from the MODIS satellite sensors, J. Geophys. Res., 113, D14S07, 2008.

Rosenfeld, D., Sherwood, S., Wood, R., and Donner, L.: Climate effects of aerosol-cloud interactions, Science, 343, doi:10.1126/science.1247490, 2014.

Savoie, D. L., Maring, H. B., Izaguirre, M. A., Snowdon, T., and Custals, L.: Ground-based measurements of aerosol chemical, physical and optical properties during the Puerto Rico Dust Experiment (PRIDE), Eos Trans. AGU, 2000.

Sayer, A. M., Hsu, N. C., Bettenhausen, C., and Jeong, M.-J.: Validation and uncertainty estimates for MODIS collection 6 "Deep Blue" aerosol data, J. Geophys. Res., 118, 7864–7872, 2013.

Scheuvens, D., Schütz, L., Kandler, K., Ebert, M., and Weinbruch, S.: Bulk composition of northern African dust and its source sediments - A compilation, Earth-Science Rev., 116, 170–194, 2013.

Sciare, J., Oikonomou, K., Cachier, H., Mihalopoulos, N., Andrae, M. O., Maenhaut, W., and Sarda-Estève, R.: Aerosol mass closure and reconstruction of the light scattering coefficient over the Eastern Mediterranean Sea during the MINOS campaign, Atmos. Chem. Phys., 5, 2253–2265, doi:10.5194/acp-5-2253-2005, 2005.

Telford, P. J., Abraham, N. L., Archibald, A. T., Braesicke, P., Dalvi, M., Morgenstern, O., O'Connor, F. M., Richards, N. A. D., and Pyle, J. A.: Implementation of the Fast-JX photolysis scheme (v6.4) into the UKCA component of the MetUM chemistry-climate model (v7.3), Geosci. Model Dev., 6, 161–177, doi:10.5194/gmd-6-161-2013, 2013.

Turquety, S., Menut, L., Bessagnet, B., Anav, A., Viovy, N., Maignan, F., and Wooster, M.: APIFLAME v1.0: High resolution fire emission model and application to the Euro-Mediterranean region, Geoscientific Model Dev., 7, 587–612, doi:10.5194/gmd-7-587-2014, 2014.

von Storch, H., Langenberg, H., and Feser, F.: A Spectral Nudging Technique for Dynamical Downscaling Purposes, Mon. Weather Rev., 128, 3664âĂŞ3673, 2000.

Vuolo, M. R., Menut, L., and Chepfer, H.: Impact of transport schemes on modeled dust concentrations, J. Atmos. Oceanic Technol., 26, 1135–1143, 2009.

Wild, O., Zhu, X., and Prather, J.: Fast-J: accurate simulation of the in- and below-cloud photolysis in tropospheric chemical models, J. Atmos. Chem., 37, 245–282, 2000.

Ziemke, J., Chandra, S., Labow, G. J., Barthia, P. K., Froidevaux, L., and Witte, J. C.: A global climatology of tropospheric and stratospheric ozone derived from Aura OMI and MLS measurements, Atmos. Chem. Phys., 11, 9237–9251, doi:10.5194/acp-11-9237-2011, 2011.

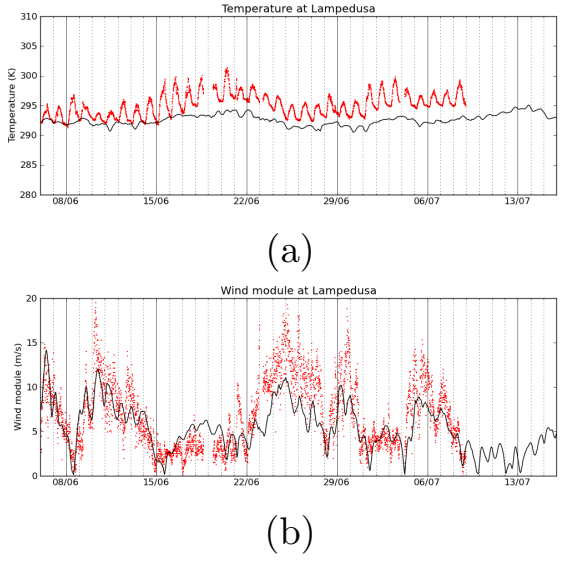

Fig. 1. (a) Modelled temperature at Lampedusa (K, black line), and measured temperature (red points); and (b), same as (a) for the module of the wind at Lampedusa (m/s).

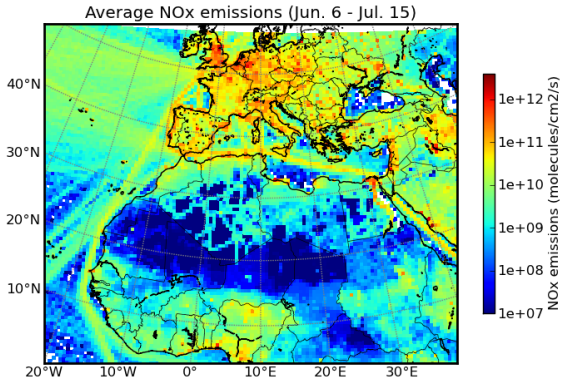

Fig. 2. Mean NO_x emissions from June 6 to July 15, in molecules $\mathrm{cm}^{-2}\ \mathrm{s}^{-1}$ as used for all three simulations

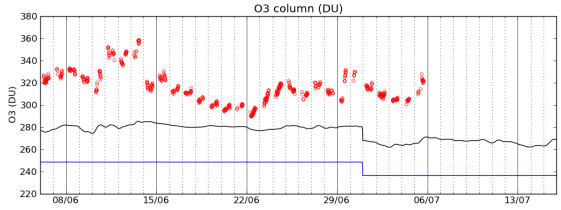

Fig. 3. Modelled total (black line) and stratospheric (blue line) ozone column above Lampedusa, expressed in Dobson Units (DU), compared to the measured values (red circles).

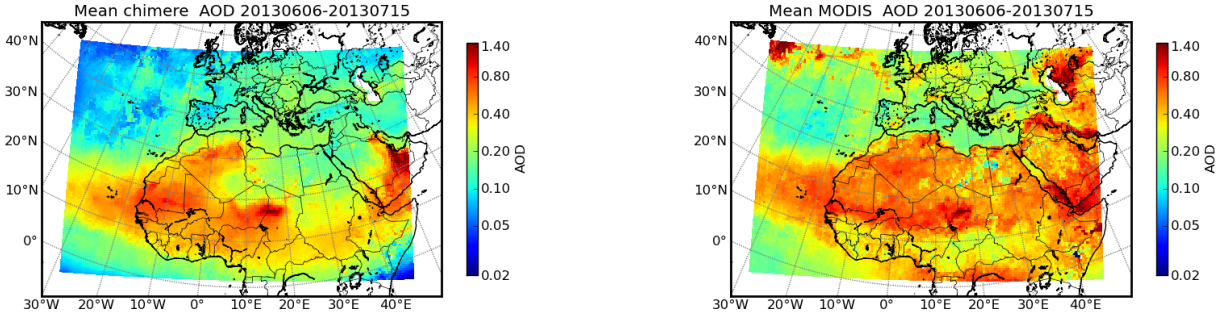

Fig. 4. AOD at 550 nm in the CHIMERE model (left column) and as observed by MODIS AQUA and TERRA, averaged from June 6, 2013 to Jul. 15th, 2013. Only the points where MODIS data are available are taken into account in the averaging procedure for the CHIMERE data.

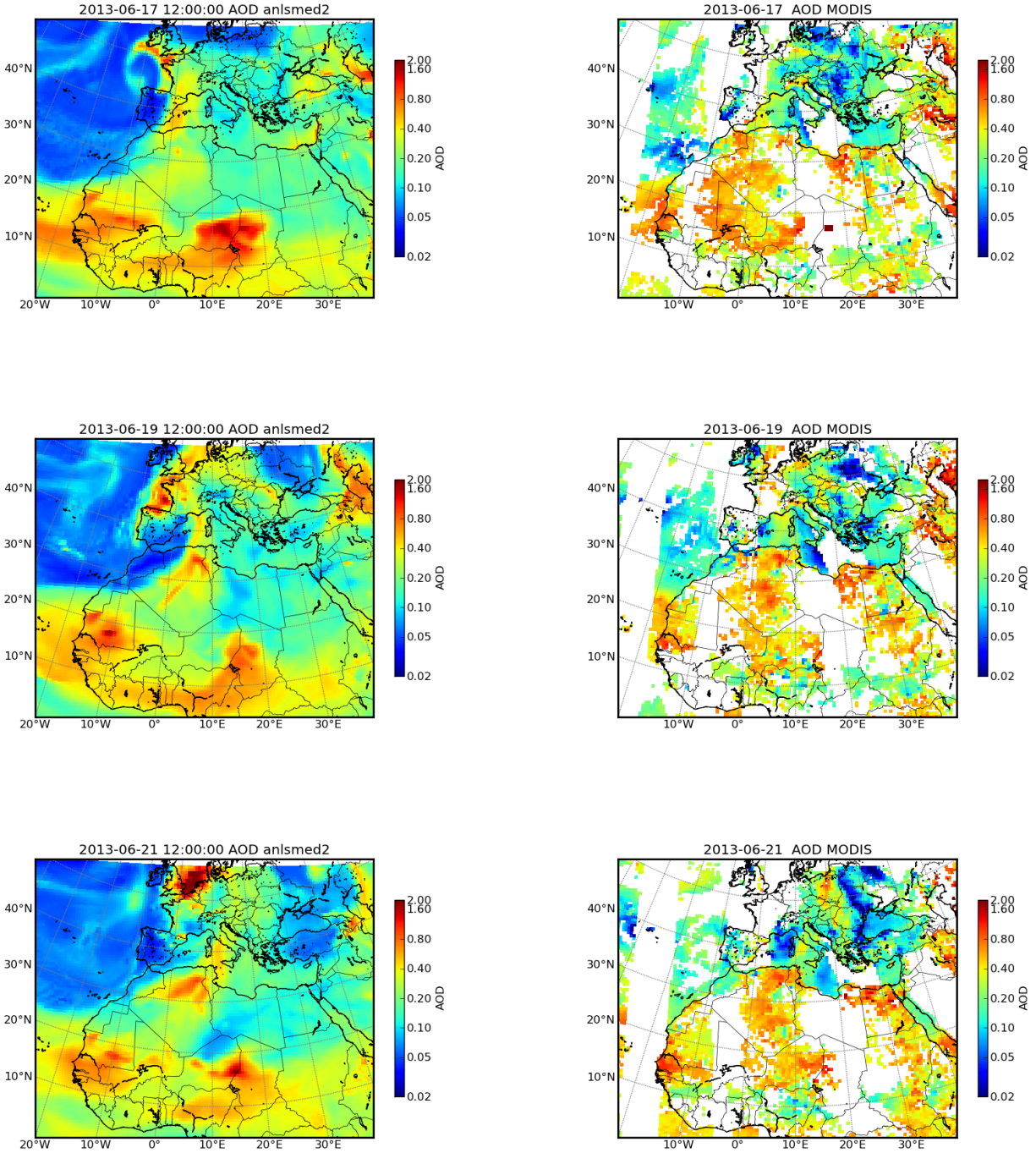

Fig. 5. AOD at 550 nm in the CHIMERE model (left column) and as observed by MODIS AQUA and TERRA, for June 17, 19 and 21, 2013.

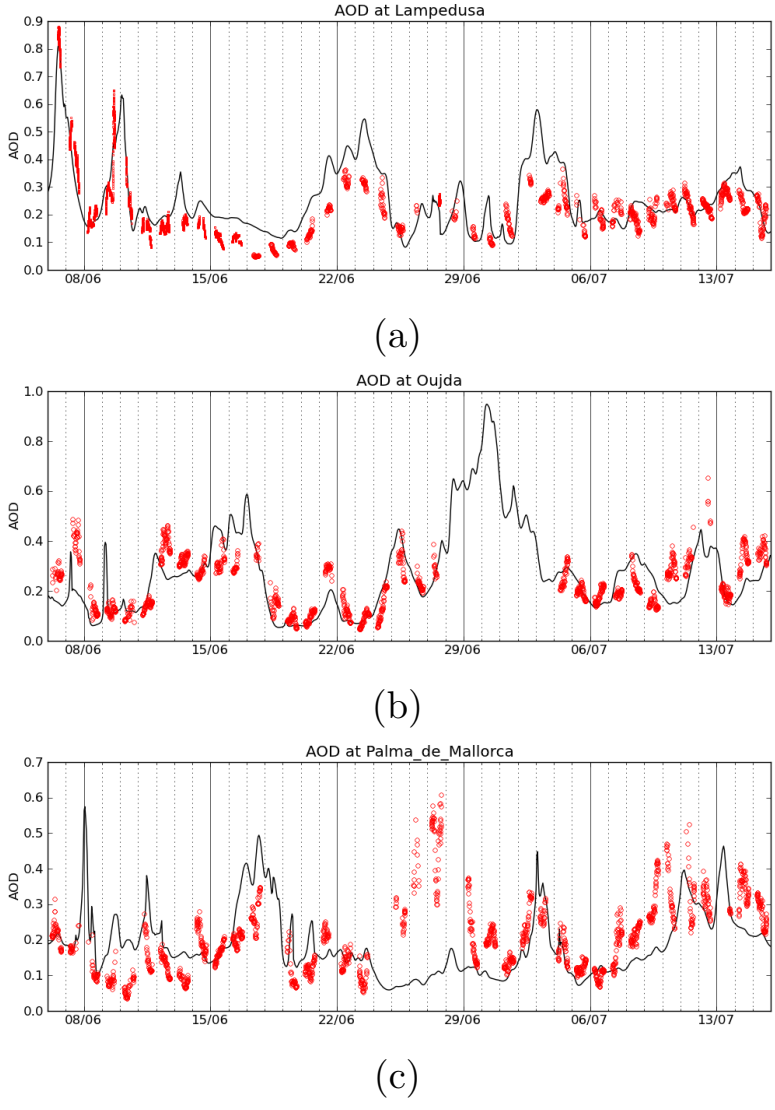

Fig. 6. Evolution of modeled AOD (black lines) at 400 nm above Lampedusa, Oujda and Palma de Mallorca, compared to the AERONET AOD interpolated at 400 nm (red circles). For Lampedusa, AERONET data is completed with MFRSR data (red dots) when the AERONET data was not available.

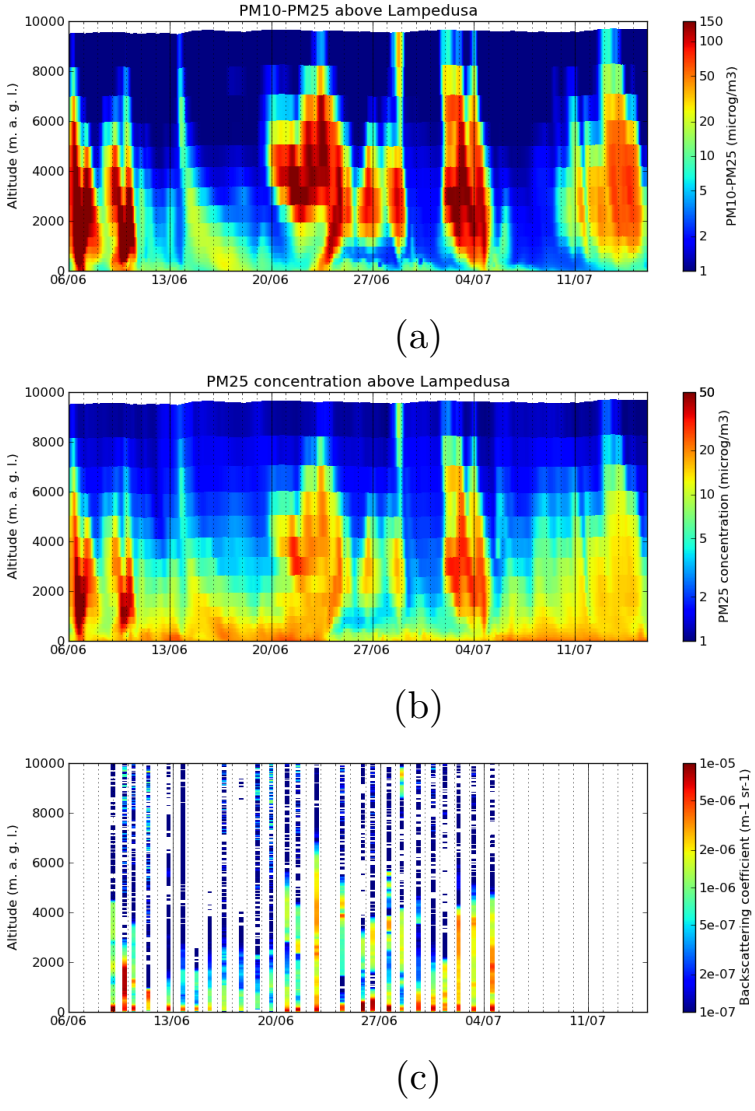

Fig. 7. (a) Evolution of modelled coarse particles concentrations (PM_{10} - $PM_{2.5}$) above Lampedusa ; (b) same as (a) but for the fine particles ($PM_{2.5}$) ; and (c) : LIDAR backscatter coefficient above Lampedusa. Each selected LIDAR profile is represented by a column of fixed width centered on the instant of the measurement, representing the backscatter coefficient (color levels).

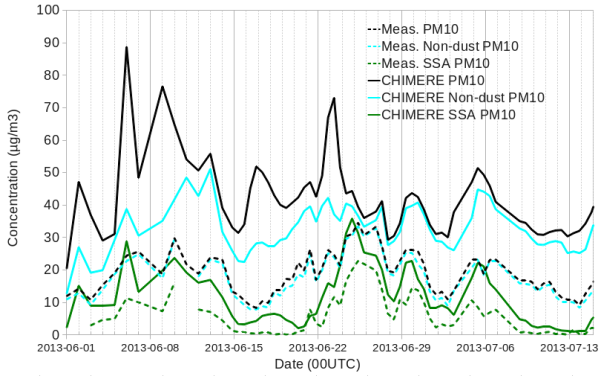

Fig. 8. Modelled speciation of PM_{10} aerosols in the first model layer compared to measurements for total PM_{10} (black lines), non-dust PM_{10} (blue lines) and sea-salt aerosols (green lines).

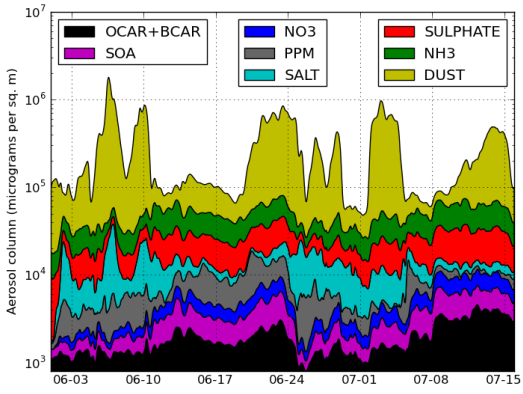

Fig. 9. Cumulative plot of the total aerosol mass load ($\mu g m^{-2}$) for the following groups of species : Organic and black carbon (OCAR+BCAR), secondary organic aerosols (SOA), nitrates (NO3), primary anthropogenic particulate matter (PPM), sea-salt (SALT), sulphate, ammonium (NH3) and mineral dust (DUST).

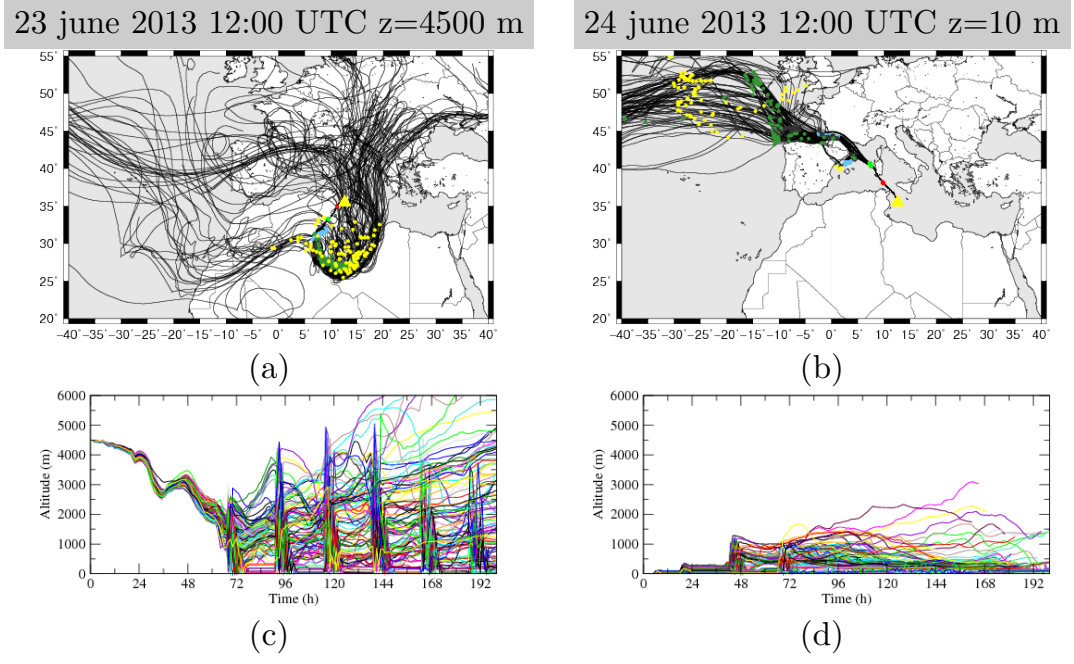

Fig. 10. (a) Backplume starting above Lampedusa for June 23, 12UTC at 4500 m altitude. The yellow triangle represents Lampedusa, the starting location of the backplume. The colored dots correspond to the number of hours before the starting time: red=12, green=24, blue=48, dark green=72, yellow=96 (b) same as (a) but for June 24, 12 UTC at 10 m altitude. (c) altitude of the backplume starting above Lampedusa for June 23, 12UTC at 4500 m altitude, and (d), altitude of the backplume starting above Lampedusa for June 24, 12UTC at 10 m altitude.

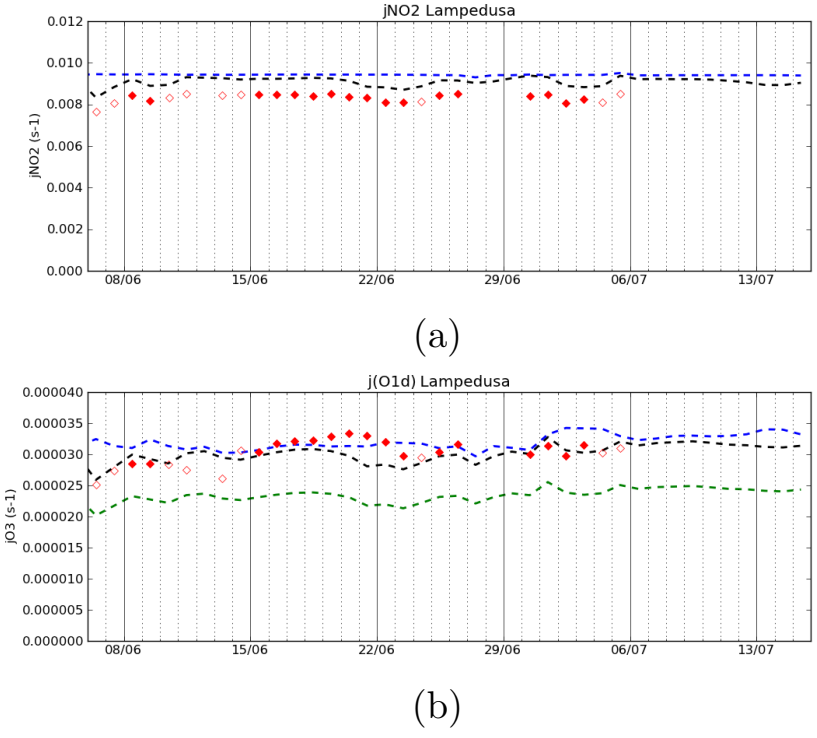

Fig. 11. (a) Daily maximal values of modelled $J(\mathrm{NO_2})$ in s-1 for the REF simulation (black dashed line) and the NA simulation (blue dashed line), and measured values of the daily maxima (red diamonds). The days when significant effect of clouds was visible on the spectrometer measurements are signalled on the plot by an empty red diamond. (b) same as (a) for $J(\mathrm{O^1D})$. The green dashed line represents the $J(\mathrm{O^1D})$ values in the *O3+* simulation.

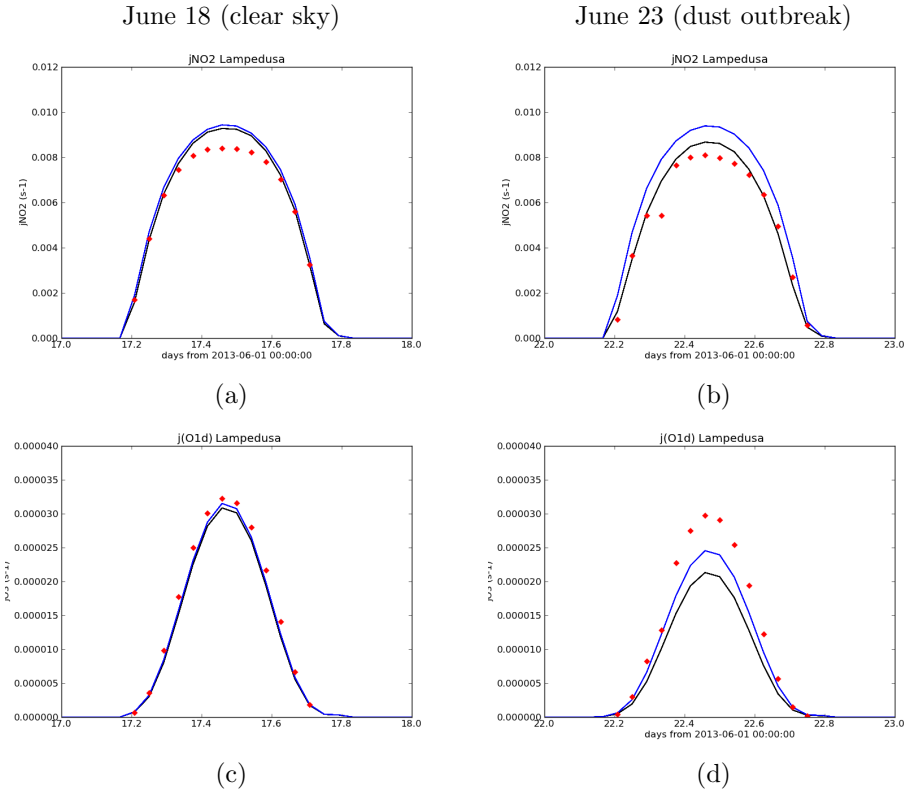

Fig. 12. (a) Hourly modelled values of $J(\mathrm{NO_2})$ in the REF simulation (black line) and in the NA simulation (blue line), and hourly measured values of $J(\mathrm{NO_2})$ (red diamonds), for June 18, 2013. (b) same as (a) but for June 23; (c): Hourly modelled values of $J(\mathrm{O^1D})$ in the REF simulation (black line) and in the NA simulation (blue line), and hourly measured values of $J(\mathrm{O^1D})$ (red diamonds), for June 18, 2013; and (d): same as (c) but for June 23.

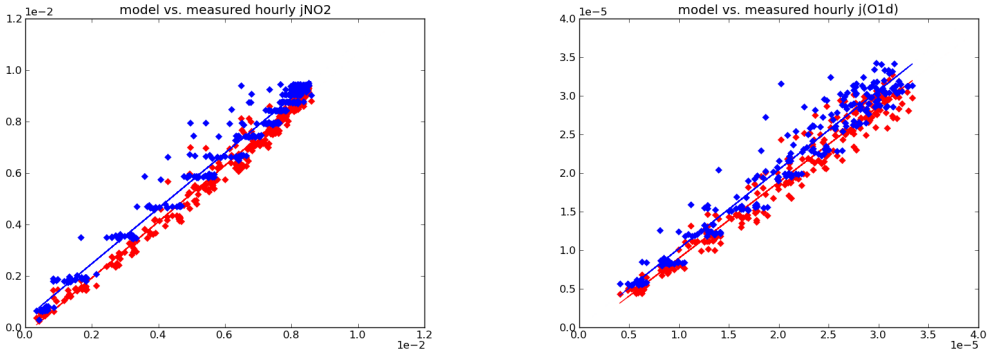

Fig. 13. (a)Scatter plot of hourly modelled $J(\mathrm{NO_2})$ versus measured $J(\mathrm{NO_2})$ at Lampedusa for 698 points with valid daytime measurements of $J(\mathrm{NO_2})$. Red diamonds represent the $J(\mathrm{NO_2})$ values in the REF simulation, blue diamonds the $J(\mathrm{NO_2})$ values in the NA simulation, with the respective regression lines ; (b) same as (a) for $J(\mathrm{O^1D})$, with 610 valid data points.

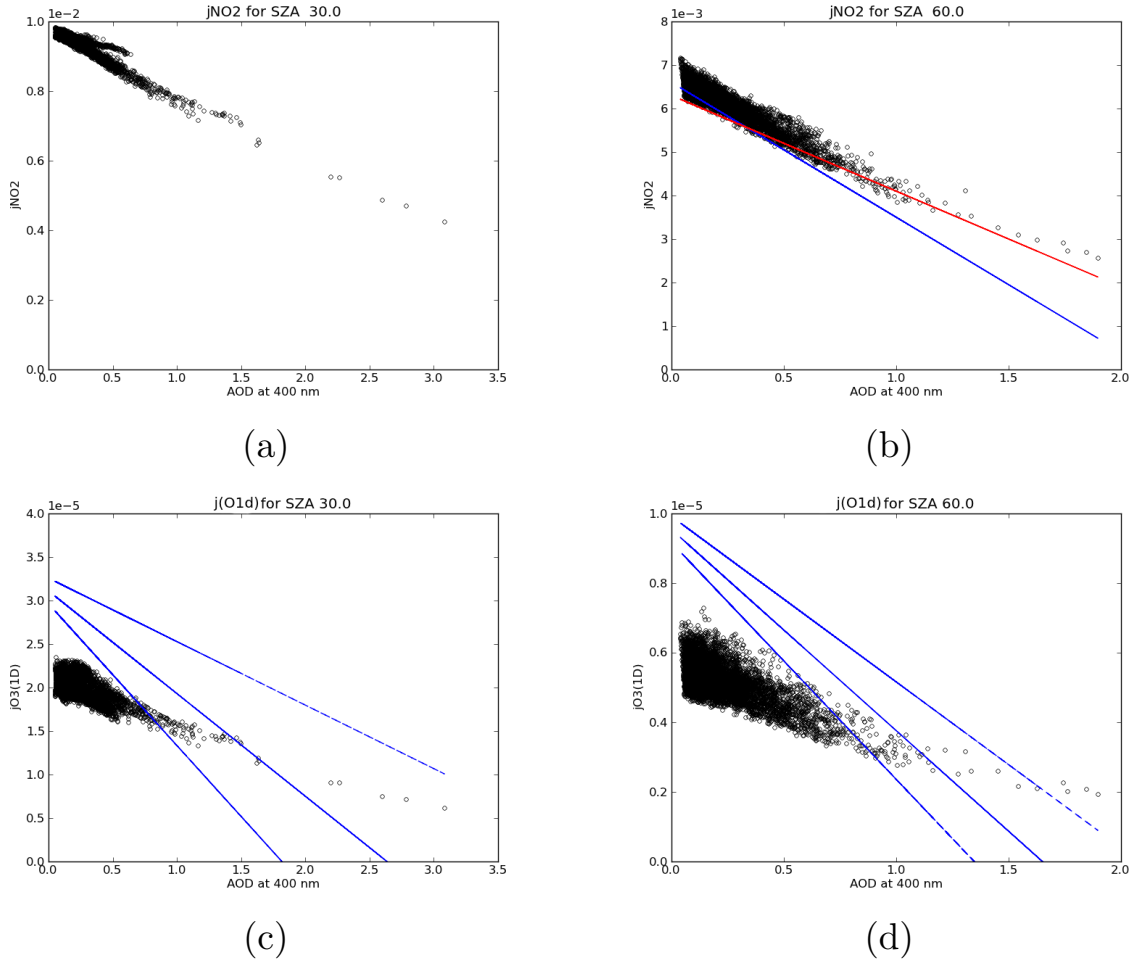

Fig. 14. Scatter plots of $J(\mathrm{NO_2})$ (a,b) and jO3(1d) (c,d) at the lowest model level versus the AOD, for clear-sky conditions ant latitudes comprised between 32.5°N and 38.5°N. For the purpose of comparison, on panel (b), the regression relationships found by Gerasopoulos et al. (2012) with field data are reported in blue (non-dust aerosols) and red (dust aerosols). On panels (c) and (d) the regression lines by Casasanta et al. (2011) are indicated along with their uncertainty margin.

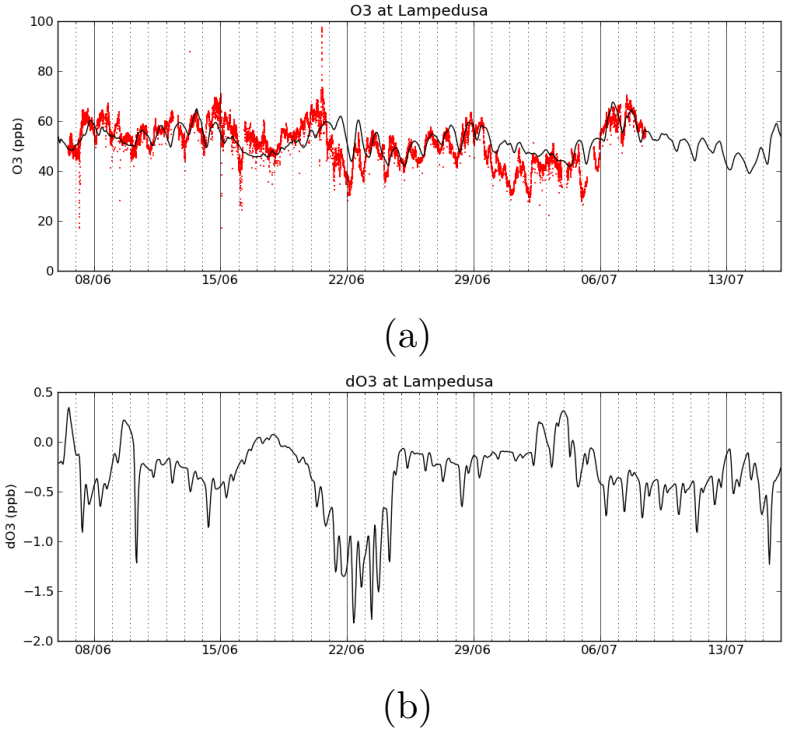

Fig. 15. (a)Time series for ozone concentration (ppb) in the reference simulation in Lampedusa (black line) along with measured values (red dots); and (b), effect of the optical screening by the aerosols on the ozone concentration, computed as $dO_3 = [O_3]_{ref} - [O_3]_{NA}$.

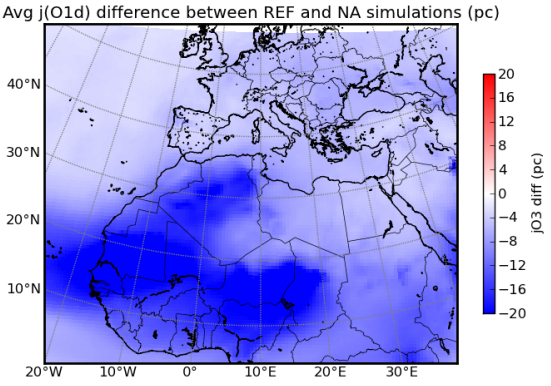

(a)

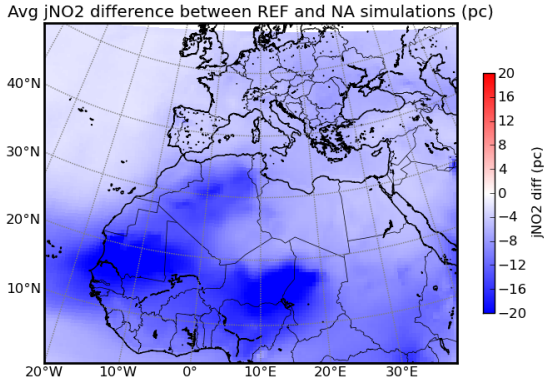

(b)

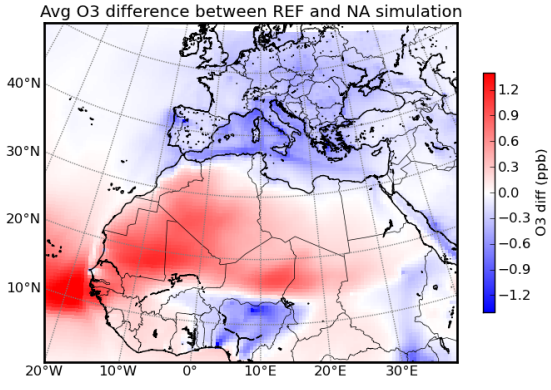

(c)

Fig. 16. (a) Average difference of $J(\mathrm{O^1D})$ between REF and NA (%) for all the simulation period (June 1 - July 15) ; (b) Average difference of $J(\mathrm{NO_2})$ between REF and NA (%) for all the simulation period ; and (c) Average difference of ozone concentration between REF and NA for all the simulation period (ppb).

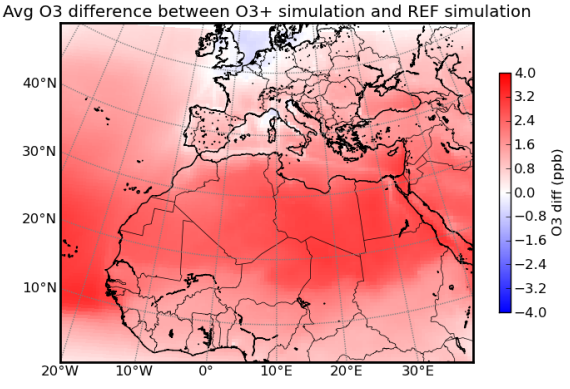

Fig. 17. Difference (ppb) in the concentration of ozone in the lowest model layer between the *O3+* simulation and the REF simulation.

bin number	Diameter range (μm)
1	0.039 - 0.078
2	0.078 - 0.15
3	0.15 - 0.31
4	0.31 - 0.625
5	0.62 - 1.25
6	1.25 - 2.50
7	2.50 - 5.00
8	5.00 - 10.00
9	10.00 - 20.00
10	20.00 - 40.00

Table 1. Sectional bins for aerosols

λ (nm)	Refractive index
200	$1.53+5.5\dot{1}0^{-3}i$
300	$1.53+5.5\dot{1}0^{-3}i$
400	$1.53+2.4\dot{1}0^{-3}i$
600	$1.53+8.9\dot{1}0^{-4}i$
1000	$1.53+7.4\dot{1}0^{-4}i$

Table 2. Refractive indices used for mineral dust.

NAME	LAT	LON	Nhour		Mean		bias	σ		R	p
			OBS	MOD	OBS	MOD		OBS	MOD		
Lampedusa	35.52	12.63	370	961	0.21	0.25	19.08	0.11	0.11	0.8	9.7e-83
Palma_de_Mallorca	39.55	2.63	440	961	0.21	0.18	-11.24	0.1	0.08	0.18	0.00011
Oujda	34.65	-1.9	377	961	0.23	0.21	-9.9	0.1	0.1	0.64	2e-45
Cap_d_en_Font	39.82	4.2	258	961	0.22	0.16	-25.12	0.11	0.08	-0.14	0.022
Gozo	36.03	14.25	461	961	0.23	0.25	8.3	0.1	0.1	0.4	5.2e-19
Murcia	38.0	-1.17	460	961	0.25	0.16	-34.23	0.12	0.09	0.36	1.2e-15
Malaga	36.72	-4.48	439	961	0.22	0.18	-16.94	0.11	0.11	0.71	3.1e-68
Potenza	40.6	15.71	339	961	0.21	0.19	-9.83	0.09	0.08	0.09	0.098
Tamanrasset_INM	22.78	-5.52	412	961	0.38	0.43	15.09	0.18	0.24	0.38	8e-16
Tizi_Ouzou	36.7	4.05	227	961	0.3	0.22	-24.63	0.12	0.15	0.51	2.1e-16
Palaiseau	48.7	2.2	202	961	0.36	0.14	-61.49	0.19	0.07	0.03	0.67
Mainz	50.0	8.3	250	961	0.32	0.18	-44.95	0.17	0.11	0.05	0.39

Table 3. Statistical scores for comparison of modelled AOD values at 400 nm (from the REF simulation) and observed ones, from AERONET network data (completed when necessary by the MFRSR data in the case of Lampedusa). For each station, the following data is given : name and geographical coordinates of the station, number of hourly values (N_{hour}), Mean value and standard deviation (σ) of observed and modelled data, correlation coefficient R and two-sided p-value for a zero hypothesis with null slope.

	$J(\mathrm{O^1D})$				$J(\mathrm{NO_2})$			
	Hourly values		Daily maxima		Hourly values		Daily maxima	
	REF	NA	REF	NA	REF	NA	REF	NA
N	490	490	26	26	578	698	26	26
slope	0.98	1.02	0.31	0.05	1.09	1.07	1.13	-0.005
R	0.981	0.972	0.46	0.09	0.993	0.987	0.92	-0.05
p	$< 10^{-10}$	$< 10^{-10}$	0.02	0.65	$< 10^{-10}$	$< 10^{-10}$	$< 10^{-10}$	0.81
Bias (%)	-5.8	+2.3	-1.8	+5.3	+4.8	+12.9	+8.2	+12.3

Table 4. Statistical scores for the regression of hourly modelled $J(\mathrm{O^1D})$ and $J(\mathrm{NO_2})$ values against measurements, for hourly values and daily maxima.